University of Copenhagen

Master's thesis

Characterizing cross-sectioned InAs nanowires for complex quantum devices

---

Author:
Daniel Ancher Ross

Supervisors:
Joachim E. Sestoft
Jesper Nygård

Center for Quantum Devices
Niels Bohr Institute

March 13, 2023

Abstract

Nanowires have attracted significant attention in recent years due to their unique properties and potential applications in various fields such as electronics and photonics. Among the different methods for synthesizing nanowires, the vapor-liquid-solid growth mechanism has emerged as a promising technique for fabricating high-quality and well-controlled nanowires. In this thesis, we relate growth of nanowires with ultra-microtomy, the technique of cutting thin sections of nanomaterials, and use this to investigate the influence of various growth parameters on the morphology, crystal structure, and composition of the nanocrystals post growth. Initially, we provide a comprehensive step-by-step guide to introduce the basics of microtoming of grown nanowires. Following, we delve into the details of sections of single nanowires, multiple merged nanowires and different types of core-shell nanowires. Here we find that we can readily cross-section not only single and multiple merged nanowires, but also different types of core-shell nanowires such as InAs/Al relevant for semiconductor-superconductor quantum devices and InAs/oxides for basic transistor devices. In the best case, we postulate that the cut face of the post-sectioned nanocrystal is cleaved leaving a very low root-mean-square surface roughness of ~ 1 nm providing enticing outlook for future device fabrication. In the worst case, we observe a detrimental shattering effect of the surface to a degree where the cross-sectioned nanocrystal are unfit for device fabrication. We dive into optimization of the microtoming process to improve yield and gain a better understanding of the key components of a successfully formed nanocrystal. Here we specifically study the cutting angle and compression effects using the electron microscopy and atomic force microscopy as the core characterizations techniques. Alternative knifeboat fluids to water are investigated seeking to adapt the microtoming process to accomadate for InAs/Pb nanowires which have been shown to be degraded by water. In the end we provide a future outlook on lamella redeposition techniques relevant for large scale nanocrystal device fabrication and single nanocrystals deposited on photonic crystal substrates as quantum dots for single photon emitters.

Acknowledgements

To begin with, I would like to express my gratitude to Jesper Nygård for inviting me to join his research group. Jesper's leadership has created a positive and supportive environment where I have felt valued and encouraged, even during the toughest times. Miķelis Marnauza, thank you for answering my avalanche of questions, even the stupid ones. You've taught me so much about electron microscopy and microtomy, and looking back, I realize that you were the best tutor I could have ever asked for (even though I may not have appreciated it at the time). Rasmus D. Scholsser, your inspiring curiosity toward any subject imaginable has left a lasting impression on me. I have yet to find a topic in which you show no interest. Daniel Kjær, thank you for being my friend over all these years. You make being squared cool. Thomas Kanne, your passion and dedication to nanowires is both impressive and a little scary, but I appreciate all that you do. I would like to thank Kasper Grove-Rasmussen and Martin Bjergfelt for always being willing to lend a helping hand when needed. Joachim E. Sestoft, a better friend or colleague does not exist. Your guidance, patience, and unwavering support have been invaluable throughout this journey. I am grateful for your friendship, even if I don't always feel deserving. Once again, I want to express my gratitude to Jesper for his leadership, and support. It has truly been a privilege to be a part of this extraordinary research group.

Lastly, I want to express my deepest gratitude to my wife and daughter for their unwavering love and support. Your patience, understanding, and sacrifices humble me. I could not have made it this far without your love and support. Thank you for always being my rock and for standing by my side. I love you both more than words can express.

Sometimes you climb out of bed in the morning and you think, 'I'm not going to make it,' but you laugh inside — remembering all the times you've felt that way. Charles Bukowski

Contents

List of Publications

Data from the following publications are included in various sections through-out this work.

- J. E. Sestoft, A. N. Gejl, T. Kanne, R. D. Schlosser, D. Ross, D. Kjær, K. Grove-Rasmussen, J. Nygård *Scalable Platform for Nanocrystal-Based Quantum Electronics.* Adv. Funct. Mater. 2022, 32, 2112941.

- Kanne, T., Olsteins, D., Marnauza, M., Vekris, A., Estrada Saldaña, J. C., Loric, S., Schlosser, R. D., Ross, D., Csonka, S., Grove-Rasmussen, K., Nygård, J. *Double Nanowires for Hybrid Quantum Devices.* Adv. Funct. Mater. 2022, 32, 2107926.

Chapter 1

Introduction

In recent years semiconductor nanowires have become an important fundamental building block in electronic and optoelectronic devices due to their unique structure, high surface-to-volume ratio and customizeable nature. As nanotechnology has evolved over the years, these structures have found their way into a host of different applications such as transistors[1, 2], optoelectronic[3, 4] and modern quantum devices.[5–7] One of the prevalent techniques used to produce these structures is called vapor-liquid-solid (VLS) growth.[8] This is a process where nanowires are grown from a metallic catalyst droplet acting as a nucleation point when exposed to a flux of the desired materials, e.g. In and As or Si. The VLS method has become particularly attractive because it allows for the growth of nanowires with controlled diameters, lengths, and crystal structures under ultra-clean conditions and ultra high vacuum.

A different technique used for nanometrology and nanofabrication is called microtromy.[9] This is a technique using a so-called ultra-microtome which cuts thin slices from a sample using a diamond blade and then allows for examination of the resulting cross-section using various (electron) microscopy techniques or for electronic and optical device fabrication. Over the last couple of years microtomy has gained popularity as a tool for cross-sectioning of nanowires.[10–16]

Recently, the combination of ultramicrotomy and VLS grown nanowires has been utilized to build a platform which produces nanocrystals embedded in resin as a new means to fabricate devices for quantum transport

experiments in an entirely different manner.[17] In this thesis, we build on the existing work[17] and seek to further investigate the structure and properties of more complex nanocrystals towards their future implementation in electronic quantum devices.

Thesis outline

This thesis is composed from three major segments. (1) A short and introductory theoretical section on the basics of vapour-liquid-solid growth of nanowires. (2) A section detailing on the application aspects of microtome operation, which starts from sample preparation and ends with how the basic characterization techniques described previously are applied. (3) In the Results and Discussion part a series of different types of nanocrystals ranging from single, multiple and multi-compositional nanocrystals and their according characterization are presented. In the end a conclusion summarizing the findings is presented.

Chapter 2

Experimental methods

2.1 Nanowire growth

The nanowires utilized in this study were grown using the VLS method, a process that allows for the growth of nanowires with controlled diameters, lengths, and crystal structures under ultra-clean conditions and ultra high vacuum.

In this process, metal seed particles, often gold, are deposited onto a growth substrate according to a predetermined design shot into the substrate by electron beam lithography. A vapor containing the material intended for the nanowires, such as indium and arsenide, is then introduced into the chamber and absorbed by the seed particle, which acts as a catalyst. As the seed particle becomes saturated, it nucleates the material onto the substrate, and the process continues as the nanowire grows from beneath the catalyst. The nanowires composition is determined by the flux of elements exposed to the chamber, allowing for engineering of the length and diameter of the nanowires.

For the purpose of creating NCs through microtomy, the ability to grow similar nanowires across an array increases the similarity of the local environment the diamond knife meets, across the sample. As a result, we are able to cross-section large arrays of nanowires with similar crystal structures/orientations at the same time. This scalability has proven valuable to the work done. By growing the structures through VLS, we are able to make small variations in the design, in order to find the optimal structures

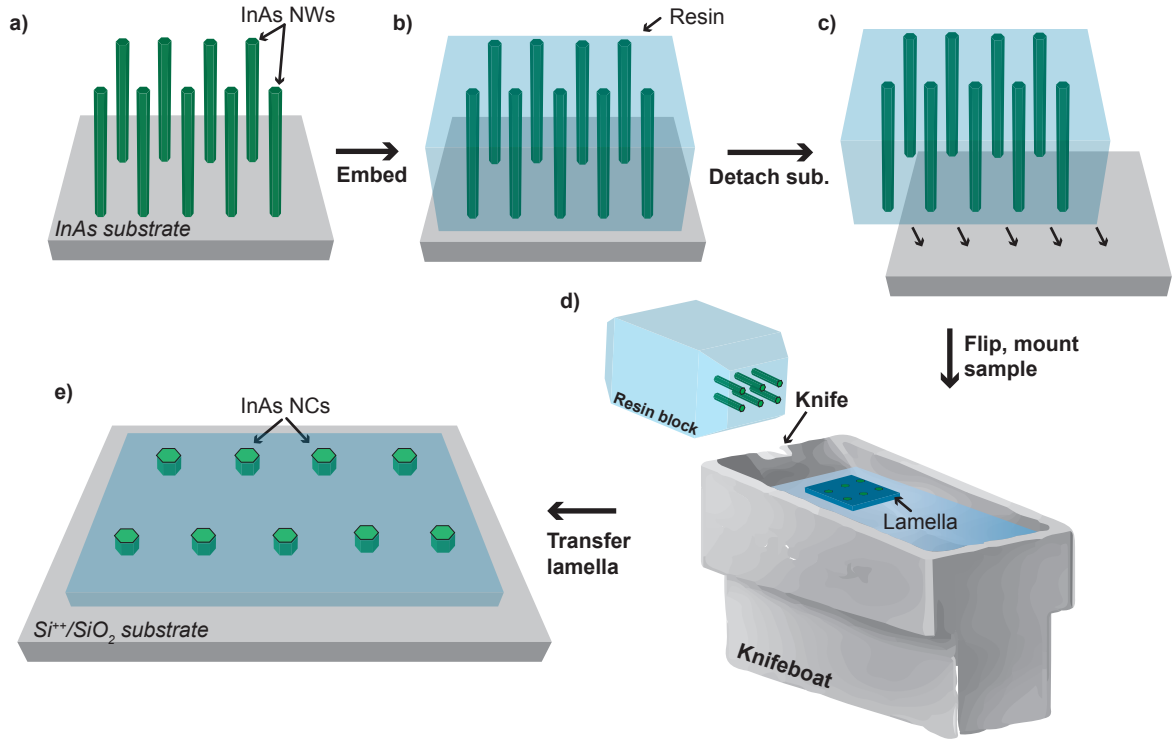

Figure 2.1: **Microtome sample preparation.** a) InAs growth substrate containing InAs nanowires. b) nanowires embedded in epoxy resin. c) Array of nanowires after embedding. d) The resin block containing nanowires mounted onto the microtome next to the knife holder. e) subsequently cut lamellas can be transferred to different substrates (e.g. a Si substrate or a TEM grid). Figure adopted from Ref.[17]

for creating ideal NCs.

2.2 Microtomy

A microtome is an instrument used in fields such as histology, electron microscopy, and materials science. It is designed to produce ultra-thin slices of a specimen such as human tissue, bone, plant material, minerals, and polymers for examination under a microscope [18]. The microtome operates by using a sharp knife that cuts the specimen into sections with uniform and precise thickness, ranging from a few nanometers to a few micrometers. The applied knives range from a homemade glass knife to a high-end specialized diamond knives, depending on the required sections thickness, hardness and

quality of the sample.

2.2.1 Sample preparation

To prepare a growth substrate with nanowire arrays for cross-sectioning using a microtome, multiple steps are performed.

Cleaving the growth substrate into smaller pieces. This step involves dividing the growth substrate, into smaller pieces that contain nanowire arrays. Cleaving the substrate is done, using a manual scriber, to make the pieces fit inside a mold for the next step.

Embedding the nanowires in resin. The next step involves embedding the nanowire arrays in resin. In the work presented here, SPURR [19, 20] is used. This is done to stabilize the nanowires and protect them during the sectioning process. The resin is poured into a mold that is designed to hold the substrate, and the resin is baked at high temperatures for a period of 24 hours to harden and cure the sample.

Creating multiple samples with different arrays. Multiple samples with different nanowire arrays are prepared by dividing the growth substrate into smaller pieces and embedding each piece in separate cavities of the mold. This allows for multiple cross-sections of the same growth to be made and studied, increasing the number of opportunities to study the growth, lowering the risk of loosing arrays due to mistakes in the sectioning process.

Removing the Growth Substrate. Before sectioning the nanowires the substrate must be removed, revealing the bottom of the nanowires to the sample surface, referred to as the block face. This process involves using a razor blade to trim away the surrounding resin and 'pop' out the substrate. Once the substrate is removed, the block face is meticulously trimmed down to only encompass the desired region of nanowires. Maintaining proper angles and steepness of the block face is vital to achieve optimal results, while any damage or contamination on the block face can pose a threat to the knife. Excessive size of the block face can also result in damage to the diamond knife

With the these steps the nanowires in the sample are protected and stabilized during the sectioning process. The sample is then mounted into the sample holder of the microtome and cross-sectioning can be performed.

2.2.2 Cross-sectioning

To obtain cross-sections of the sample, the sample is mounted onto the microtome such that the diamond knife is positioned at a perpendicular angle to the blockface. It is essential that the blockface of the sample is correctly aligned with the diamond knife for the quality of the cross-section. This alignment process is a manual procedure that requires skill and experience to avoid damaging either the sample or the diamond knife.

Moving the blockface of the sample in close proximity of the knife edge, a reflection of the knife edge can be seen, by looking through the inbuilt microscope of the microtome, on the blockface which is used as a guide for aligning. If the reflection distorts as the sample is moved from above to below the knife edge, alignment must be done. To achieve optimal alignment, the knife holder in the setup can be carefully tilted in the horizontal or vertical plane, respectively. To avoid any potential collision that may damage the knife or the blockface, the sample must be retracted to a safe distance away from the knife during the tilting process. This precaution is essential in ensuring the safety of both the sample and the diamond knife. The tilting process should be done with utmost care and precision to obtain good cross-sections of the sample. Proper alignment is crucial to ensure that the cross-sections obtained are accurate and precise, and that the microtome setup is not damaged during the process.

One of the important considerations when choosing the size of the blockface is the tradeoff between the size of the blockface and the quality of the resulting sections. As the area of the blockface decreases, the quality of the sections generally improves. Big blockfaces risk damaging the knife when sectioning. There is a limit to how small the blockface should be made, as it can become difficult to see the knife edge reflection when aligning the sample. In this work, the microtome used is not designed for blockfaces below 500 μm^2. This means that aligning the sample can be challenging, as the knife edge reflection may be difficult to observe. In some extreme cases,

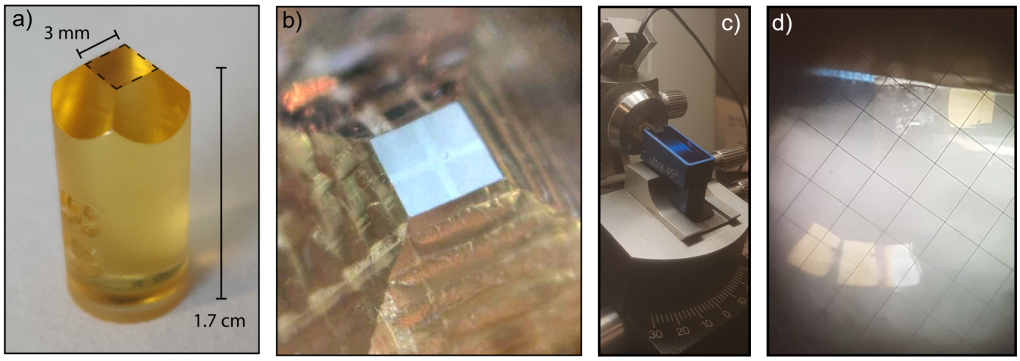

Figure 2.2: **Microtome Process.** a) blank microtome sample bullet. The dimensions of the height and block face area illustrated on the picture. b) Trimmed blockface containing four nanowire arrays. The area is $\sim 220\ \mu m^2$. c) Microtome alignment configuration. d) Cross-sections floating ontop of the water surface of the knifeboat, seen through the microtome microscope. Three sections are forming a ribbon while a single lamella is at the knife edge.

the inbuilt microscope can not reach a high enough magnification to see the reflection on the blockface. In such situations, the operator can choose to align the sample "blind" without being able to see the knife edge reflection. It requires a high level of skill and experience, as the operator must rely on their knowledge of the microtome and alignment to achieve accurate and precise results.

After achieving successful alignment, it is important to set the cutting speed and increments of advancement towards the knife using the microtome control panel. This step requires careful consideration of factors such as sample hardness, knife quality, and blockface size to avoid defects such as section compression, chatter, wetting of the blockface, or thickness variation. For the sectioning method presented in this work, a cutting speed of 1.4 mm/s at increments of 70 nm is recommended as a general rule of thumb. The microtome control panel sets a nominal thickness through the advancement length between cuts.

Once sectioning is complete, the sections are suspended on the water surface in the knifeboat. The sections' color, which relates to the interference between the section and the water surface, can be used to estimate their thickness with better accuracy than the nominal value set on the microtome

control panel. A color table [21] can be referenced to achieve this. The color table provides enough information to indicate if a section's thickness is below 100 nm, which makes it suitable for TEM investigation. Actual measurements of section thickness can be obtained using AFM scans. If the sectioning went well the resulting cross-sections appear in a ribbon, floating on the surface of a water filling the knifeboat. The right volume of water used in the knifeboat is essential to have the right surface tension, ensuring that the cross-sections remain intact until and during the transfer process onto a substrate such as a TEM grid, Si chip or another suitable substrate. The transfer process is a delicate process that requires precision to avoid any damage to the cross-sections. One of the risks during the transfer process is that the ribbon-like sections may collapse onto themselves or the surrounding environment. This can result in significant damage to the cross-sections, and once the damage is done, it cannot be undone. Care must be taken to ensure that the cross-sections remain intact during the transfer process. To guide the sections floating on the water surface during sectioning or to remove contaminations such as dust or oil particles from the water medium, a custom tool is created by attaching an eyebrow hair to the end of a small wooden stick, resembling a "fishing rod". A rough and fine variation of this tool are made by gluing the eyebrow hair either with the thick bottom part facing toward or away from the rod. An image of such a tool can be seen in the appendix Figure 5.1(a-c). To prevent contamination, the fishing rods are used only for a single round of sectioning, and new ones are made before mounting a new sample onto the microtome.

Transferring sections onto a TEM grid is done by carefully lowering the grid down towards the section in the knifeboat, making sure not to break the water tension. As the water connects with the grid, a droplet containing the section will transfer onto the grid as it is removed from the knifeboat. The water is then removed by capillary suction into a filter paper, and the section is deposited on the TEM grid ready for investigation. A specialized tool called *Perfect loop* [22], seen in the appendix Figure 5.1(d-e), can be used for transferring to TEM grids when only a few sections are present in the knifeboat. Transferring to other substrates such as a Si substrate is done by submerging the substrate partially into the water and guiding the section onto the substrate using above mentioned eyebrow tool. This

is challenging and can be incredibly frustrating, especially when trying to transfer a section to a fixed location, like between bonding pads of a chip.

2.3 Aligning Nanocrystals in TEM

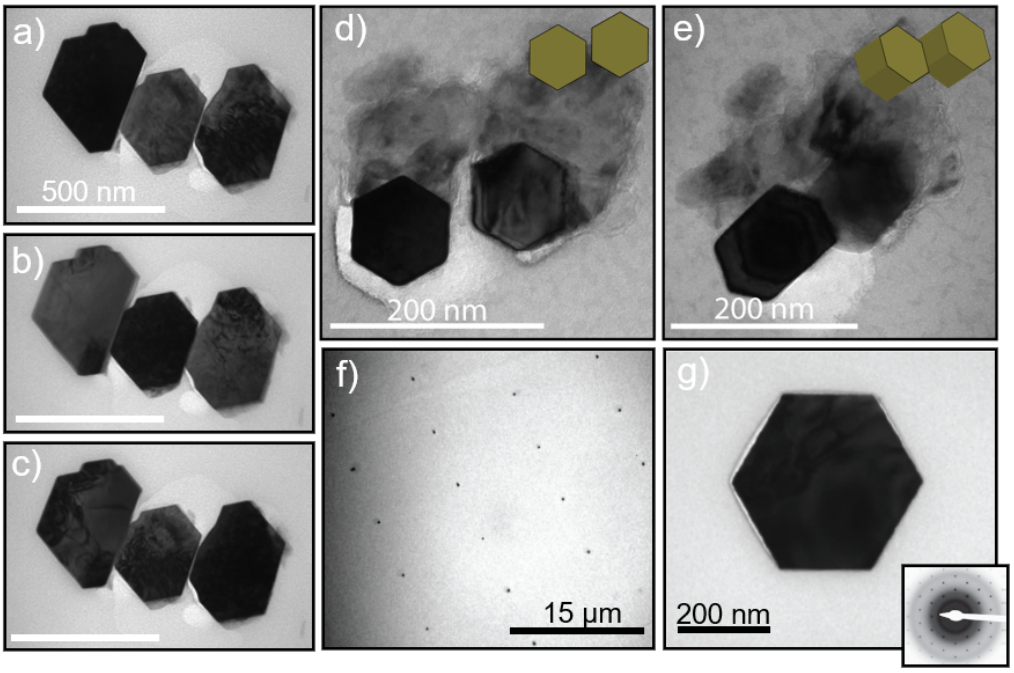

Figure 2.3: **Alignment of nanocrystals in TEM.** a-c) Three NCs grown next to each other. The micrographs are aligned to each individual NC from left to right respectively. The scale bar is 500 nm for all of them. d-e) A pair of parralel InAs NCs with a half shell of Al deposited onto their facets. An illustration of their orrientation respectively is portrayed in the top right corner. f) An Array of NCs transferred to a TEM grid. g) TEM micrograph of a single NC. In the lower right a SAED is seen showing the intact crystallinity of the NC.

Using a TEM, diffraction patterns and micrographs of a crystal can be gathered. The electron beam needs to be aligned with a high symmetry orientation of the crystal to get good results. This is achieved by using Kikuchi lines [18]. Kikuchi lines are formed as a result of incoherent electron scattering in the crystal. By using the Kikuchi lines as a guide, the crystal can be tilted into a high symmetry orientation, relative to the column beam.

Thicker samples makes this process easier as the signal from the scattered electron of a certain type is stronger, this is an important factor when investigating NCs in TEM, since they typically are of a lower thickness relative to the full length nanowire laying on the side. In practice Kikuchi lines guide the operator, by going into reciprocal space, the Fourier transform of real space, while converging the electron beam onto the crystal. The diffraction pattern of a crystal is the projection of the reciprocal lattice, in which each spot denotes to a set of crystallographic planes. By converging the beam, the incident electrons incoherently scattered over a range of different angles. They are then Bragg diffracted [18] by the crystal planes of the lattice resulting in a convergent beam electron diffraction (CBED) pattern. From the CBED pattern, the crystal structure and orientation of the nanowire or NCs can be determined.

When nanowires are grown in arrays, they are not identical to one another, as each individual wire has a unique local environment that can result in variations in its structure, such as strain, micro-faceting, and stacking faults. Aligning one NC to a high symmetry orientation does not guarantee that its neighboring NCs will also be aligned. In Figure 2.3(a-c) an example of this can be seen, having the different NCs aligned in each their micrograph. With the size of the NCs and the close proximity of each other, getting the beam converged onto a single NC and not the others is often not possible using the on site low-resolution 200 kV Philips-FEI CM20 large tilt TEM. This results in having to navigate the Kikuchi lines, while also getting a signal from the other crystals, which are in a different orientation. The NCs are typically of a thickness that makes this process harder as to compared to a full length nanowire laying on the side. Another important step when investigating NCs is to make sure that they are aligned to the high symmetry zone axis, along the growth direction, since other high symmetry orientations drastically changes the apparent structure of the NC. Figure 2.3(d-e) show an example of two different high symmetry orientations of two parallel NCs. One of the challenges in studying NCs through TEM is the limited capabilities of the microscope. In this study, a low-resolution TEM was used, which means that locating the NCs can be time-consuming due to their small size. Even when the NCs are easily located, difficulties can arise when attempting to align to a specific NC,

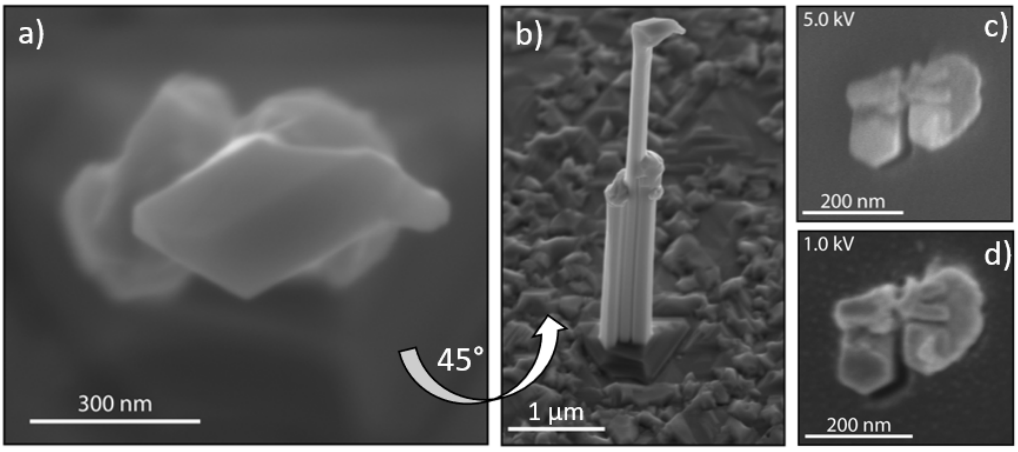

Figure 2.4: **SEM investigation of nanowires and nanocrystals.** a) SEM image of three as-grown InAs nanowires vievew from a the top. b) SEM image of the three as-grown nanowires, with a 45° tilt of the sample holder scan the structure along the length of the waires. c-d) SEM image of two parallel grown InAs nannowires, with a Al shell on the facets seen in the top. The images are taken with a 5 kV and 1 kV acceleration current respectively, giving different resolutions of the surface.

as physically tilting the sample holder inside the column cause the sample to shift position, making it challenging to maintain a fixed position on the targeted NC. Figure 2.3(f-g) show an array of single InAs NCs. These NCs are hard to distinguish, meaning during alignment, the operator risks losing track of the NC aligning to, and mistake another NC for the first.

2.4 Nanocrystal and nanowire imaging using SEM

To obtain images of as-grown nanowires using SEM, the growth substrate was tilted by 45°, unless otherwise indicated. This enables investigation along the entire length of the nanowire by producing a projection of its structure. By applying the equation below, the actual height of the imaged structure can be determined

$$L_{\text{real}} = L_{\text{projected}} \cdot \sin^{-1}(\theta) \tag{2.1}$$

where L_{real} and $L_{\text{projected}}$ is the real and projected length of the nanowire while the tilt angle is denoted by θ.

Once the sample has been cross-sectioned and transferred onto a substrate, the created NCs are of thicknesss below 100 nm. Figure 2.4(c-d) show the effect of lowering the acceleration voltage in order to better probe the morphology of the surface structure.

Chapter 3

Results and Discussion

In this section we will step through the various species of characterized nanocrystal structures ranging from single nanocrystals, through multiple connected nanocrystals as well as different types of core-shell nanocrystals.

3.1 Exploring different approaches to sample preparation

Nanowires with a full shell of Al or Pb have proven a challenge to detach from the growth substrate, and in these cases submerging the sample into liquid nitrogen to then remove the growth substrate has worked (Thermal expansion etc).

3.1.1 Sectioning nanowires with atomic layer deposited oxides

InAs nanowire hybrids using Pb as the superconductor has shown not only does Pb contain the highest bulk critical temperature T_C it also have other properties making it an interesting alternative to using Al as the superconductor. At deposition temperatures below 150 K, it becomes energetically favorable for Pb to grow in a single crystallographic orientation in respect to InAs. This is due to the low thermal energy available to break growth symmetry. Combining the single orientation with the high grain boundary mobility of Pb, it is likely that a large crystal formation with

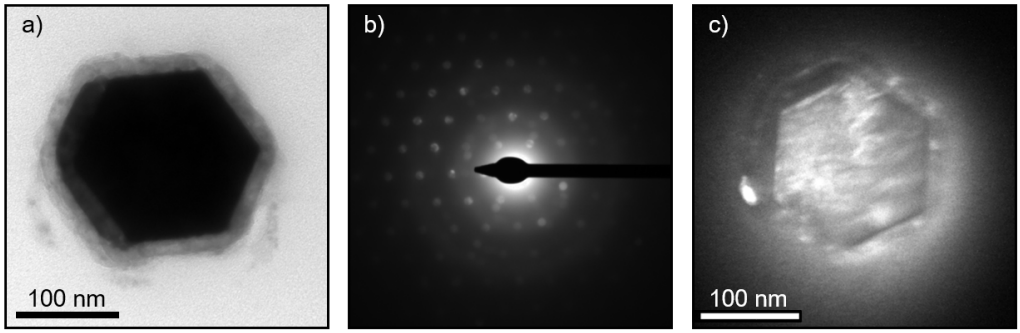

Figure 3.1: **NC containing Pb.** a) TEM micrograph of a 150nm thick InAs NC, with epitaxial Pb deposited on two facets followed up by a full shell of epitaxially deposited Al. b) SAED of the NC, showing the presence of Pb. c) Dark-field TEM micrograph of the NC. This NC were created using microtomy by Miķelis Marnauza, and used with his permission.

an epitaxial match to the InAs nanowire will grow along the facet. The high mobility of Pb at grain boundaries is caused by its low stacking fault energy [23], permitting different orientations to merge into a single crystal [24]. Epitaxial grown Al grow in two to four different orientations on InAs depending on the thickness [25]. This could become a problem, not only for devices fabricated with these structures, but also for NCs. A big obstacle for using epitaxial grown Pb on InAs NCs is caused by H_2O acting as an etching agent to the Pb thin films [24].

Previous attempts to make NCs from these nanowires failed due to Pb being etched away, presumably by H_2O in the knifeboat of the diamond knife. Figure 3.1 show that it is possible however. The NC is made of a core of InAs, a 10 nm wide layer of Pb on two facets and a full shell around the structure of Al. To prepare the sample for TEM investigation, the approach of sectioning the sample at a thickness of 150 nm was used, which had the potential risk of damaging the diamond knife as well as the sample being too thick for TEM observation. The NC containing Pb post sectioning was achieved by quickly transferring the newly sectioned lamella onto a TEM grid and placing it in a vacuum. The presence of Pb in the sample was confirmed by observing it in both the bright-field and dark-field micrographs, as well as by detecting its signal in the SAED pattern.

Attempting to perform cross-sections at smaller thicknesses led to the

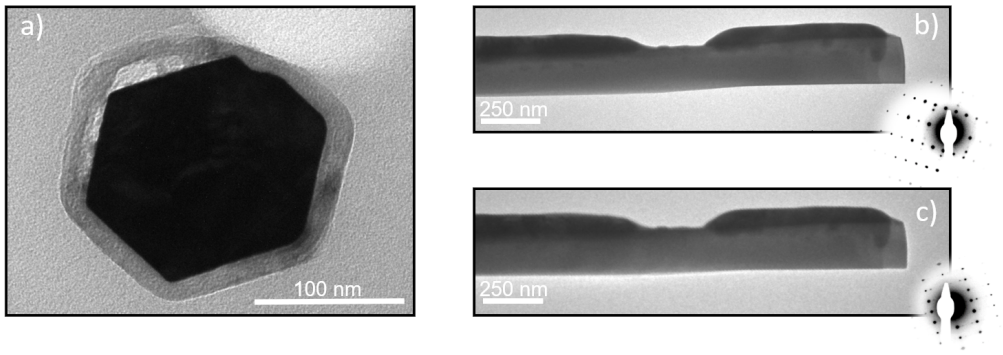

Figure 3.2: **Producing NCs containing Pb.** a) TEM micrograph of an InAs NC, capped in a shell of HfO_2 deposited through ALD. The two facets that had Pb deposited on the nanowire, are bare post sectioning. b) TEM micrograph of an InAs nanowire with two facets containing 50 nm Pb. The microgaph is aligned to the facet of the wire. Bottom right inset show a color inverted SAED of the wire in which Pb is seen. c) TEM micrograph of the nanowire after it was submerged in butyl acetate for 40 s. Bottom right inset shows a SAED of the wire in which Pb still is present.

loss of Pb in the NCs. Furthermore, most of the NCs on the successful lamella were devoid of Pb, suggesting that this method is not dependable. To investigate other means of obtaining NCs with epitaxial Pb on InAs, an alternative approach was explored using atomic layer deposition (ALD) to deposit a complete oxide shell, shielding it from the environment.

HfO_2 and AlO_2 were deposited separately onto a growth substrate of InAs/Pb nanowires to compare the quality of cleaving between the two oxides. The aim of this investigation was to examine the potential of passivating the surface of the structures by using a protective layer of oxide, similar to the epitaxially grown Al shell, and to evaluate the effectiveness of the microtome setup in sectioning a sample that had undergone the ALD process. Both oxides proved to be 'section'able with no difference in the quality of the cut between the two. No sections were performed above 100 nm thickness for the ALD treated samples, due to the risk of the knife, showing wear and tear at this stage. A TEM micrograph of a NC with a shell of HfO_2 is shown in figure 3.2(a). The section quality has no difference when compared to sections done without the ALD process, but no Pb was found across those NCs. ALD has proven a compatible tool combined with

microtomy, and future work exploring how to utilize the two techniques is highly encouraged.

3.1.2 Using Butyl Acetate as knifeboat fluid

With the knowledge that NCs containing Pb can be obtained through microtomy by making sections with thicknesses above 150 nm, another tactic was investigated. While H_2O etches the Pb away, it is reported that acetone leaves the Pb intact[24]. Using acetone as the knifeboat medium is not practical for two reasons. The first issue is caused by the acetone reacting with the glue binding the diamond knife to the knife holder, ruining the tool. Even with a knife capable to use acetone as the section medium, the evaporation time of acetone would make it extremely hard to keep the right surface tension in the knifeboat, needed for sectioning. Butyl acetate has an evaporation rate closer to H_2O than to acetone, but should react similarly to acetone. To test this, a TEM grid was prepared with InAs/Pb nanowires, and submerged for 40 seconds into butyl acetate. Individual wires were caratherized by TEM before and after the exposure to butyl acetate to see if the fluid has any etching effect on the Pb. Figure 3.2(b,c) show that the Pb film show no sign of reacting with butyl acetate.

After obtaining an alternative adhesive material from a manufacturer (Syntek) along with a diamond knife specifically designed for non-H_2O mediums in microtoming, the epoxy was tested for its suitability for the task. One key concern was whether it would react with butyl acetate, a potential replacement for H_2O as a sectioning medium. The epoxy was subjected to a 20-hour exposure to butyl acetate, with no significant effects observed, as shown in Figure 5.3 in the appendix. After the test, the butyl acetate was rinsed off the sample with MilliQ water and then dried with nitrogen.

In addition to testing the effects of butyl acetate on the epoxy, the effects of butyl acetate on other materials used in the microtoming process were also investigated. The microtome resin showed no significant damage from 15-minute submersion in butyl acetate, as shown in Figure 5.2 in the appendix.

Next, the effects of butyl acetate on TEM grids and cross-sectioned lamellas containing NCs with thicknesses below 100 nm were investigated.

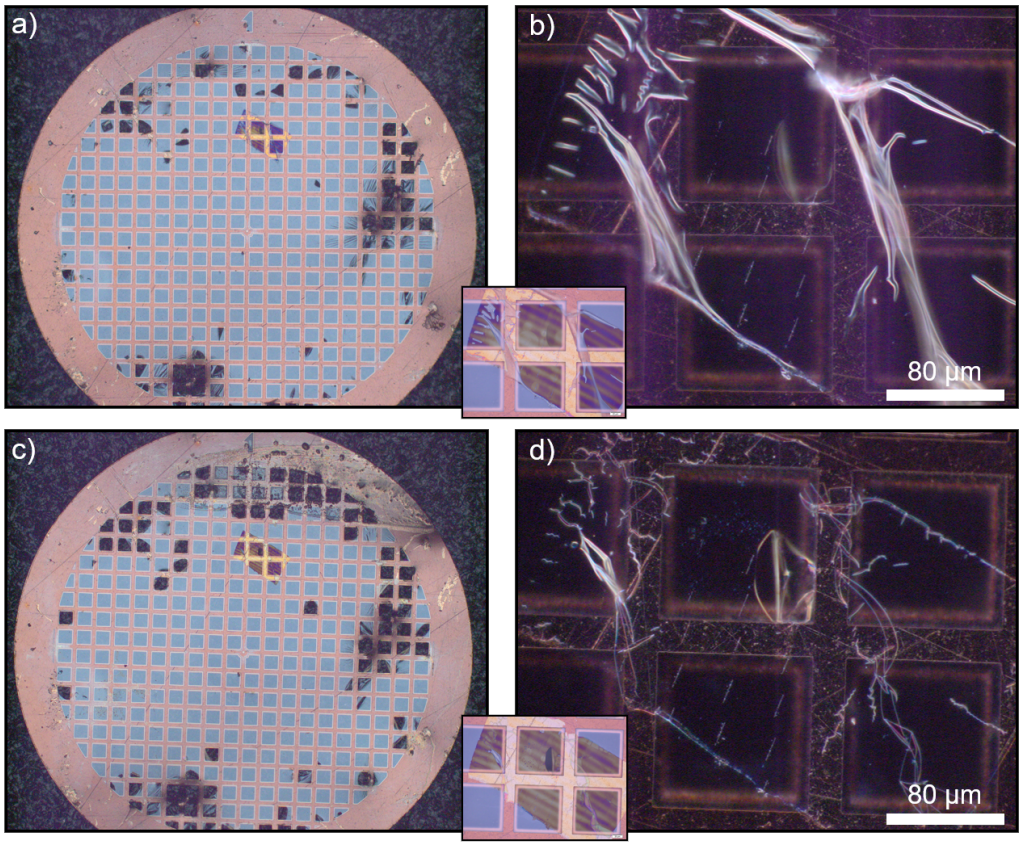

Figure 3.3: **Section on TEM grid exposed to butyl acetate for 5 minutes.** Optical images of TEM grid with cross-section lamella . The sample was submerged into butyl acetate for 5 minutes to simulate the time a lamella will spend floating on the knifeboat medium before getting transfer ed to a sample. a-b) Sample before submerged in butyl acetate. b) Sample after submersion in butyl acetate. The two insets in the lower left of (b) and (d) is the bright-field image of the dark-field image shown.

A TEM grid containing a lamella with NCs was submerged in butyl acetate for 5 minutes, and the effects were observed. Figures 3.3(a-b) show the TEM grid prior to the test, while Figures 3.3(c-d) show the effects after 5 minutes of exposure, followed by rinsing with MilliQ water and drying with nitrogen.

The TEM grid and the lamella containing the NCs showed no signs of damage, an interesting phenomenon occurred. Figure 3.3(b,d) show folds and wrinkles of the lamella contracts as a result of this process. Controls were performed to TEM grids with NC lamellas from the same sample as previous one were, with no exposure to butyl acetate, rinsed and dried following the same protocol. Controls that underwent the same rinsing and drying process showed no change in their folds and wrinkles. This suggests that the contraction observed in the lamella was not caused by the rinsing or drying process, but instead has something to do with the butyl acetate itself. One possibility is that the lamella contains pockets of water residue from the knifeboat medium that were trapped underneath it during the transferring phase. Submerging the sample into butyl acetate may have caused the trapped water to be replaced by the butyl acetate. Unlike water, the butyl acetate does not appear to get trapped in these cavities and instead diffuses away during the rinsing and drying phase.

To create InAs/Pb/Al NCs, microtomy using butyl acetate was performed once, with a custom knife holder used to attach the diamond knife via the alternative epoxy mentioned earlier. The process was challenging due to the butyl acetate reacting with the plastic parts of the microtome, making any spill during operation potentially damaging to the machine, and operator. The resulting NCs had a section thickness of 60 nm. TEM characterization revealed that the InAs core and Al shell were intact, but no Pb was present in any of the NCs, despite no exposure to water. One possibility is that the epitaxially grown Pb reacts with the water in the air when it is cleaved. To test this, a microtome setup that allows for control of humidity levels would be necessary.

3.1.3 Characterizing the same nanocrystals

The track-ability of NCs across multiple types of investigation tools is important in order to ensure control over the structures as the sectioning

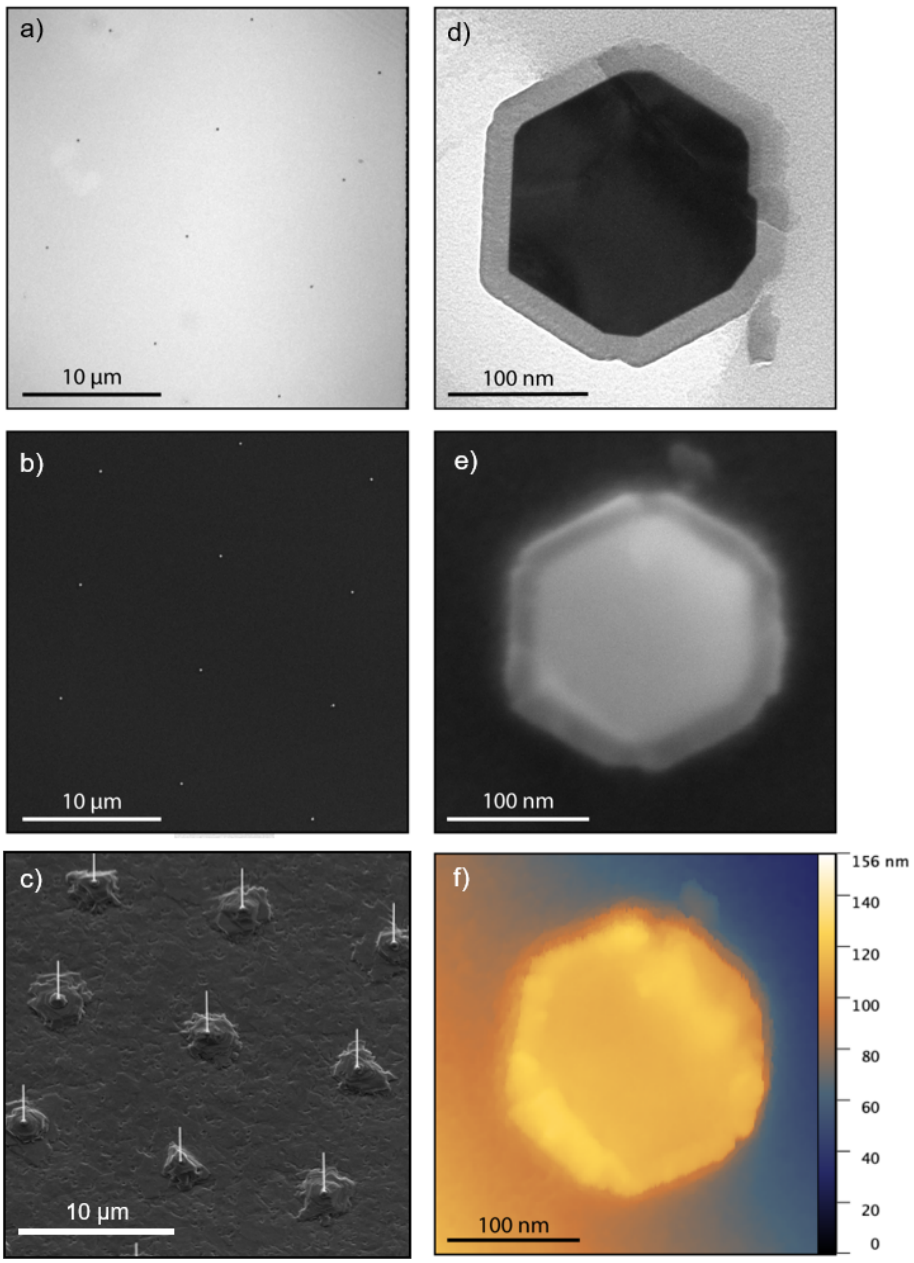

Figure 3.4: **Multiple methods of investigating the same nanowire NC: TEM, SEM, and AFM.** a-b) TEM and SEM, respectively, images of the same NC array. c) SEM image of the NC array on the growth substrate prior to sectioning. d) TEM micrograph of the center NC in (a). e) SEM image of the center NC in (b). f) AFM data of the NC seen in (e). Note that the NC in (e,f) is the section following the one for (d) meaning they are made from the same nanowire, with no length of wire between them.

process proceeds. Figure 3.4 shows how the same nanowire NC is studied both through TEM, SEM, and AFM. Note that the TEM NC is transferred onto a TEM grid, and the following lamella was transferred to a $Si^{(++)}/SiO_2$ substrate, which is investigated by SEM and AFM. The overview panels show the scalability of the method, and the ability to investigate an as-grown nanowire before sectioning it.

Even though the TEM NC is not precisely the same as the one in the SEM and AFM panels, it is the direct neighbor. This is evident from the corners of the Al shell, which show the same microfaceting across the two NCs. The consistency in the microfaceting between the two NCs indicates that they are adjacent to each other and belong to the same nanowire. Figure 3.4 highlights the importance of having access to different investigation tools to gain insights that are not accessible from any single one of them. Panel e) of the figure shows a NC with sharp facets that provide information about the morphology of the surface material. The non-conducting resin surrounding the NC does not send any signal to the SEM detectors, making it impossible to gather data about whether the NC is embedded into the resin or protruding from it.

From the AFM data, it is seen that the NC is indeed sticking out of the lamella. It is important to note that these sections were done at a thickness of 100 nm. The substrate with the lamella is mounted onto a piece of carbon tape, which causes the substrate surface to be tilted in respect to the cantilever. Adding to this, the lamella is not lying perfectly flat on top of the already slightly tilted substrate, leading to a slope that falls from the bottom left to the top right of the AFM scan. While this can be corrected through the AFM software, the raw data is shown in the figure to best represent the ability to investigate the same NC with different tools.

These results demonstrate the importance of using multiple investigation tools to obtain a more comprehensive understanding of nanowire structures. While each tool has its own limitations, using them in combination can reveal information that is not accessible from any single tool alone.

3.1.4 Using TEM, SEM and AFM on the same nanocrystals

In order to acquire data from all three of the investigation techniques mentioned above for the same NC, the transferring the lamella to a TEM grid is required. The compatibility of the TEM grid with the two other techniques provides some complexity. Figure 3.5 demonstrates that it is possible to perform SEM on a TEM grid, and also AFM scans were performed to the sample showing no issues between the TEM grid and the AFM cantilever.

Mounting the TEM grid onto carbon tape for the SEM and AFM investigation, resulted in some bending of the grid from pulling with a tweezers to unmount the sample again. Furthermore the SEM investigation left the TEM grid with noticeable carbon deposition. The fragility of a TEM grid compared to a Si/SiO_2 substrate vastly shortens the life time of the sample. despite these challenges, using a TEM grid for all three investigations enables a comprehensive study of the same NC.

One useful thing that was learned from performing SEM on a TEM grid was the ability to visualize NCs that are located on top of the copper grid. These NCs are not accessible using TEM, as the grid copper prevents transmission through the NCs. This problem has previously caused significant frustration. The ability to access these otherwise hidden NCs on a TEM grid using SEM provides a valuable alternative method for investigating their morphology. This finding highlights the importance of using multiple techniques to obtain a more comprehensive understanding of sample structures, particularly in cases where certain techniques are limited if only the conventional methods are used.

The ability to perform SEM on a TEM grid provides a more efficient and streamlined approach to investigating NC structures for characterization, but it also limits the possibility for device fabrication with the NCs.

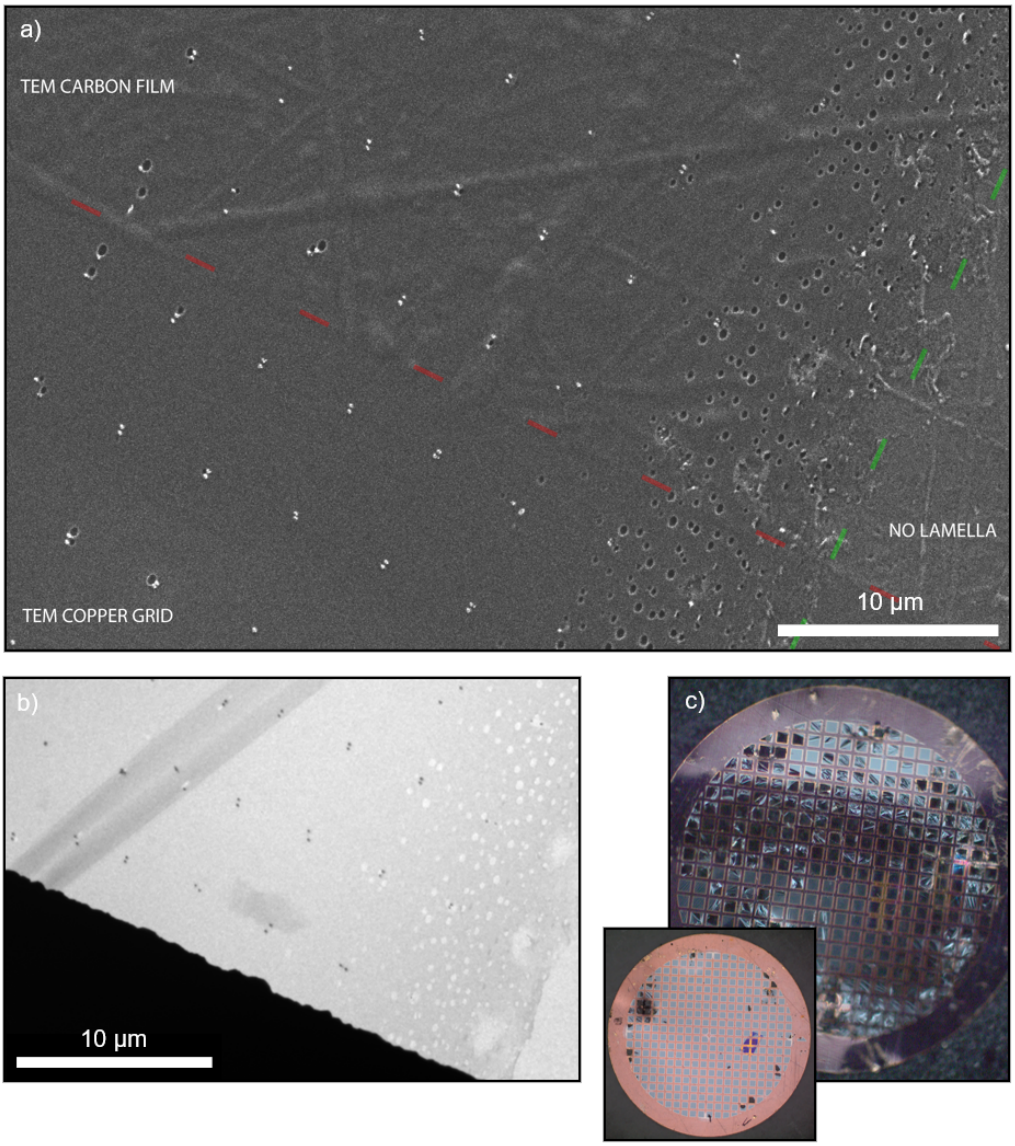

Figure 3.5: **Lamella of a InAs parallel NCs array transferred onto a TEM grid.** a) SEM image of an array of NCs transferred to a TEM grid. Above the dashed red line is the carbon film of the TEM grid, while beneath the line is the copper grid on which the carbon film is suspended between. The dashed green line indicate where the lamella with the NCs (left). b) TEM micrograph of the same sample. Note that the are of a) is not the same area as b) of the NC array. c) An optical image of the TEM grid after it was investigated by SEM. The inset in the lower left show the TEM grid prior to the SEM investigation contrasting the effects of SEMing onto the sample.

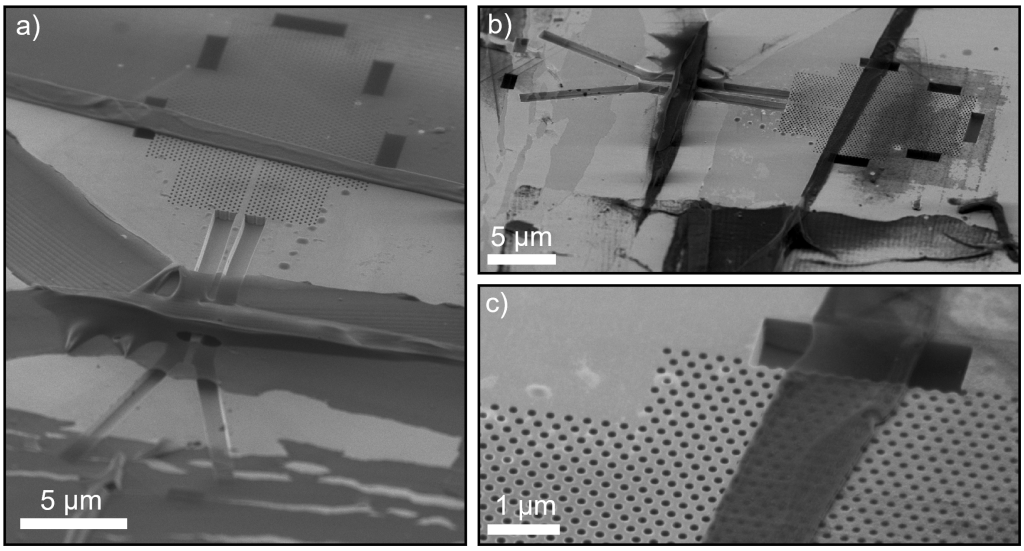

Figure 3.6: **Ashing lamella void of NCs.** a) SEM image of transferred lamella to regions of a chip. Holes in the lamella where NCs were embedded. b) Same area as seen in (a), after 8 minutes of oxygen plasma etching. c) zoom onto the folded lamella that still remains after ashing, but gone from the sides.

3.1.5 Ashing of resin lamella

A ribbon of 19 consecutive cross-sections containing NCs is seen in Figure 3.8. A blockface of ($\sim$ 70 x 70 µm) was prepared to ensure the quality of the sections despite having a complex configuration of nanowire structures. The small block face made it impossible to align the sample through reflections due to the limitation of magnification on the microtome, instead relying on the operator's experience. The result of the sections here is a long segment of consecutively cut nanowire structures into NCs. This means that not only can the array of NCs be studied in respect to each other, as seen in Figure 5.5, but also in respect to themselves along the length of the nanowires, seen in Figure 3.9. All eight structures were tracked over the same consecutive sections, the remaining NCs seen in the appendix Figures 5.7-5.13. Some top facet of the NCs appear to have cracks and signs of shattering, previously observed in samples with poorly grown wires and less than optimal cross-sections as a result of misalignment and similar variables. No significant sign of bad sectioning can be found on the lamella,

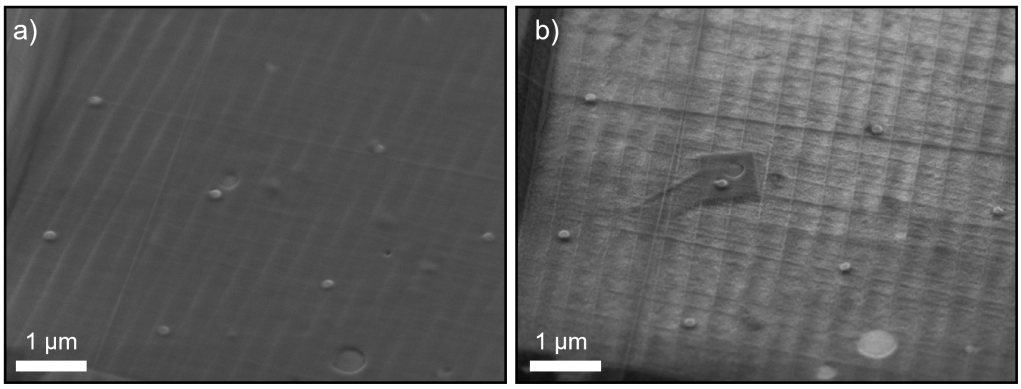

Figure 3.7: **Ashing stacked lamella of resin with NCs.** SEM image of two lamellas, transffered at with a 90° rotation relative to eachother. This is seen from the criss-cross of the ridges. The top lamella contains an array of NCs. a) prior b) after 8 minutes of oxygen plasma etching.

meaning that the cross-sectioning was performed really well. NCs sectioned from nanowires in simple configurations such as parallel grown or single wires show that we are able to achieve NCs with a flat surface from where the knife cleaved the crystal. AFM data from one such wire is seen in the appendix Figure 5.5. A line trace is measured across the NC, parallel with the tilt of the sample, to show the raw data of the protruding NC. The InAs core of the NC is then used to calculate the root mean square roughness of the surface. The roughness is calculated to be $\sim$ 1 nm. For the complex structure of NCs, while the lamella is good (note that the fold running across the lamella is typical for sections cut at 70 nm and below), the top facet to have plateau like structuring tilted in respect to the lamella surface. Locally the top facet roughness is low, but steep declines breaks up the surface. Figure 3.11 show a region investigated through AFM (a) and SEM (c). The data set is shown as a overlay in (d), the white arrows showing the direction from which the knife cut.

While the top facets of the NCs are rough, it is likely that the NCs have smooth facets on the side. This is because a small misalignment relative to a crystal plane could mean that the wire still cleaves along the crystal plane, until too much stress from the knife is met, terminating the crystal plane cleave into step-like formations.

The resin the NCs are embedded into can be removed by oxygen plasma

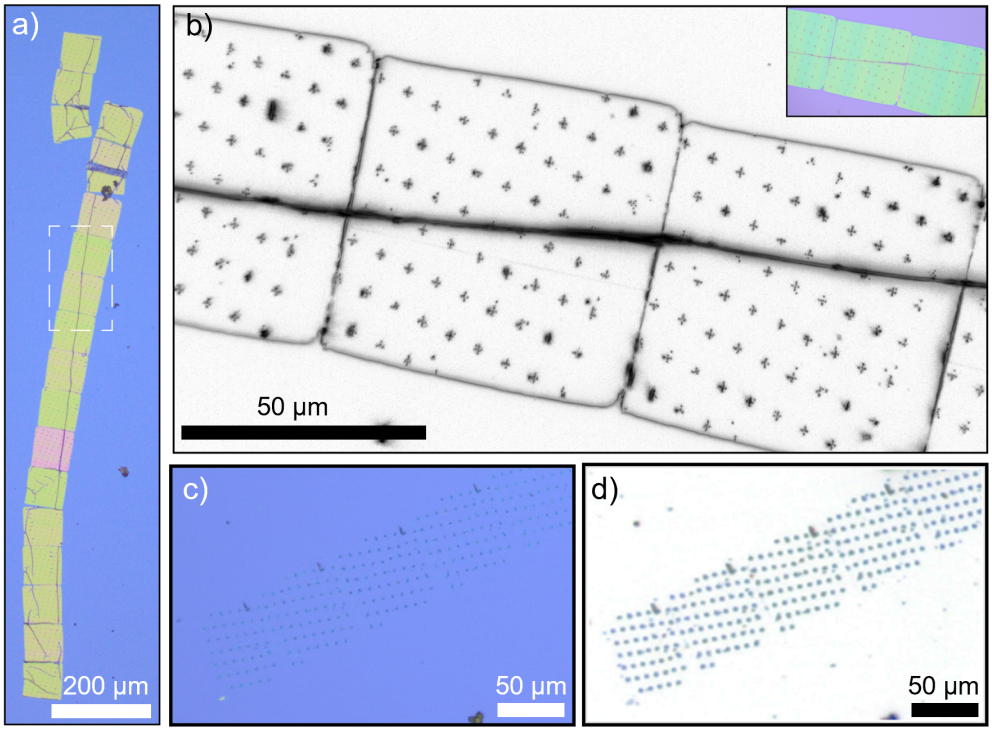

Figure 3.8: **Ribbon of sections containing NCs.** a) Optical image transffered ribbon of sections with NCs. The sections in the bottom of the frame are of the bottom wire, progressing higher along the length of the wire with each section upward. b) a magnified optical image of the area seen marked with a white border in (a). The image is an inverted dark-field image, increase the contrast of the structures in the array. Inset in top right is of the same area, in the form of a bright-field image. c-d) Bright-field(c)/inverted darkfield(d) optical image of the sample after oxygen plasma etch. The resin removed without moving the NCs configuration.

ashing. Figure 3.8 (c-d) show an optical image (bright-field and dark-field) of sections after 18 minuts of ashing at 100 W. Ashing can remove the bulk of the resin. Some residue remains present after ashing though, regardless of how long the lamella is exposed to ashing. Figure 3.7 show a ribbon of lamellas transfered ontop a chip structure. (a) show the region prior to ashing, and (b) show the same region after 8 minutes of oxygen plasma ashing done in segments of one minute to avoid hardbaking the resin. A zoom on a folded part of the lamella is seen in (c) showing how the layering the resin on top of it self, or with other lamellas, vastly cripples the ability to ash it away. Two stacked lamellas are seen in Figure 3.6, the top lamella contain-

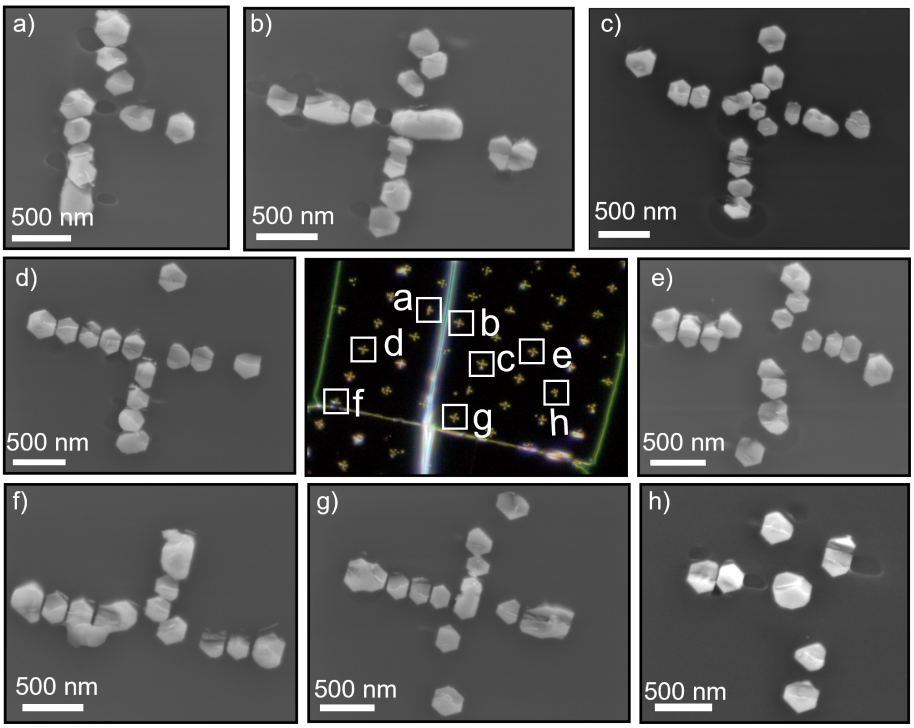

Figure 3.9: **NCs from a complex structured nanowire array across a cross-section.** a-h) SEM images of NCs in different cross-like configurations. In the middle an optical image of the lamella is seen, indexing the location of each of the show structures using the same indexing as the figure format.

ing NCs. The lamellas were transffered such that they lay perpendicular to each other in respect to the cut direction. small ridges in the lamella can be seen, which is common. The thickness variation due to the ridges, remain after ashing. The ashed image reveal clearly the ridges from that lamella, creating a grid-like image of the surface. The NC in the middle of the SEM images was investigated locally, and the effects of SEMing onto a small region is seen by the writefield being baked into the resin. We report finding these hardened resin areas consistently with SEM exposure. The purpose of these ashed samples is shown in the appendix Figure 5.4. We aim to show that arrays of NCs can be obtained and transferred onto structures for future devices. In this case as waveguides for a photonic device.

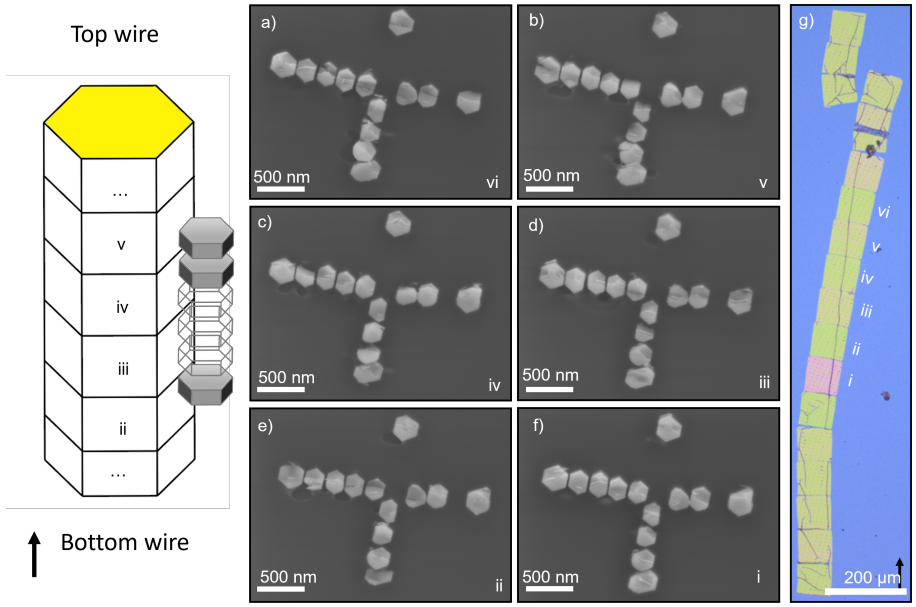

Figure 3.10: **NC configuration [d] across multiple consecutive increments.** Left: simplefied illustration of a single nanowire - portrayed as stacked NCs. On the right the nanowire is seperated into the NCs to illustrate the coherency of the NCs. The bottom left arrow indicates that the cross-sectioning is done from the bottom of the nanowires and up. a-f) SEM images of a NC structure created from the same nanowires at consecutive heights of the structure. moving down the length of the wire from (a) to (f). The index in the lower right show the order of which the NCs were performed aswell as the lamella on which they are located in (g). The [d] in the tittle, indicates the position of the structure relative to the middle panel of Figure 3.9.

3.2 Characterization of various cross-sectioned nanowires

3.2.1 Microtome capability on structures with changing hardness.

As a part of the process to test the capabilities of obtaining NCs through microtomy using nanowire structures, core-shell structures with changing materials were sectioned to see the effect of the changing resistance met by the diamond knife during a cutting window. A cutting window the period in which the diamond knife cleaves a microtome sample. We find that even for nanowires with complex disorganized stuff going on in the shell and

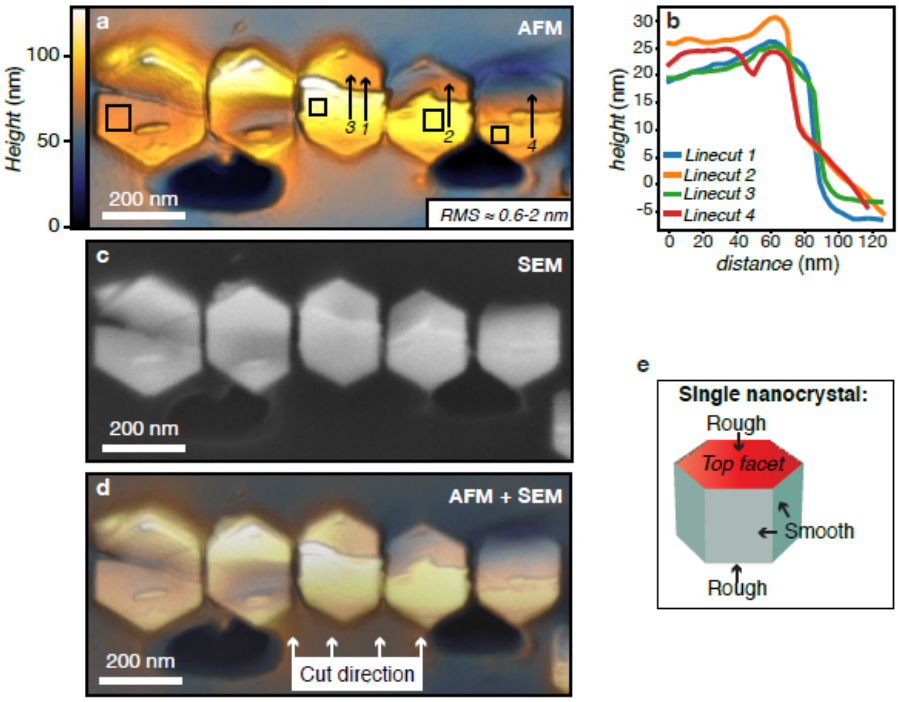

Figure 3.11: **AFM inspection of the cut face quality.** a) AFM image of a series of closely spaced NCs fixated in a lamella. Black boxes indicate where the RMS roughness of 0.9-2 nm is obtained. b) Height versus distance showing the profile along the linecuts in (a). c) SEM image of the same structure shown in (a). d) A combination of the AFM image shown in (a) and the SEM image shown in (c). White arrows illustrate cutting direction. e) Illustration of a single NC where top and bottom facets are roughened after sectioning and the six other remain pristine. The figure and figure caption is published as supporting information to the article Ref. [17]

on the outer facets, the inner layers/core remain undamaged as a result of the cross-sectioning. Figure 3.12 show some of the exotic structures that were sectioned to see if the core of the NCs would be damaged from the so rounding environment.

3.2.2 Targeted NC configurations

This section shows the ability to target specific configurations of NCs by SEM investigation of the as-grown nanowire arrays, which then can be sectioned and located/manipulated with precision. For the work below, we wanted to have three NCs physically coupled at the corners in a line. The

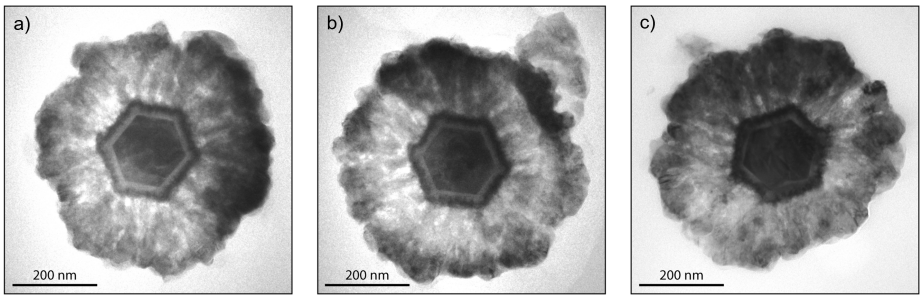

Figure 3.12: **NCs with changing composistions.** Bright-field TEM micrographs of NCs. The structures are made from an InAs core with hexagonal sharp facets, a)

NCs needed to from individual nanowires. This means that if the nanowires used had merged into a single crystal, they are considered one structure instead of multiple. If the nanowire structures are too far apart, it is easy to discard them from a preliminary SEM investigation, due to the spacing between them, which can be seen by imaging the wires from rotating angles. If however the structure is in close proximity to the neighboring wires, but not physically coupled, it is not always possible to get that information prior to sectioning.

An array with multiple candidate structures was embedded into a microtome sample. Figure 3.13 show the array prior to sectioning. 46 structures in the array were mapped out. An example of this process is found in the appendix Figure 5.14. While the time invested for the preliminary work seems high, we found that by doing so, we could obtain NCs matching our specification at a with a 0.5 accuracy. The ability to map out an array prior to sectioning and target with precision NCs for device fabrication will prove a valuable tool for future work. We note that with a yield of half the initial candidates, we have 23 NC structures on each of the lamellas. As such, devices based on the same configuration can be fabricated along the different lamellas, or, as devices with different local parameters can be made from each section. We stress that this technique requires experience, due to the many steps along the process which would destroy the sample.

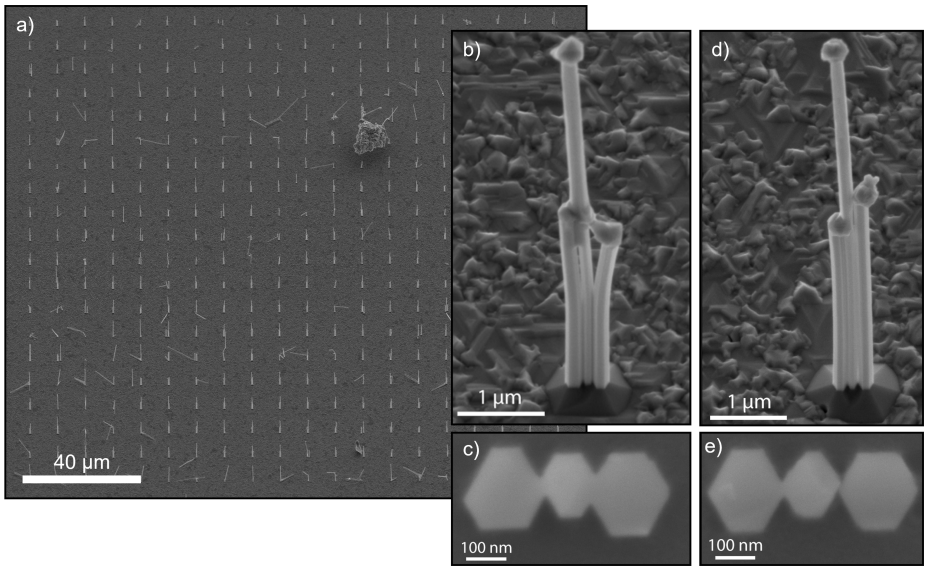

Figure 3.13: **Targeted microtomy through SEM investigation.** a) SEM image of a nanowire array. b) Candidate structure for targeted NCs prior to cross-sectioning. c) Resultinig NC from the structure in (b) showing the wires are coupled at the corners. d) Candidate structure for targeted NCs. e) Resulting NC from the structure in (d) showing that the midle and right wire are not physically coupled.

Chapter 4

Conclusions

In conclusion, this thesis has investigated microtomy of VLS grown nanowires. A comprehensive step-by-step guide to microtoming of nanowires was provided, and different types of nanowires, including single nanowires, multiple merged nanowires, and core-shell nanowires, were investigated. The results show that the cut face of the post-sectioned nanocrystal has a low surface roughness of around 1 nm, making it a promising candidate for future device fabrication. However, some post-sectioned nanowires showed a detrimental shattering effect, rendering the nanocrystals unfit for device fabrication. The optimization of the microtoming process was investigated to improve yield and gain a better understanding of the key components of successfully formed nanocrystals. This included the study of cutting angle and compression effects using electron microscopy and atomic force microscopy. Alternative knifeboat fluids to water were also investigated to accommodate InAs/Pb nanowires, which are expected to be degraded by water. Future outlooks on lamella redeposition techniques for large-scale nanocrystal device fabrication and single nanocrystals deposited on photonic crystal substrates as quantum dots for single photon emitters were provided. Overall, this thesis provides a selection of contributions to the understanding and optimization of the growth and microtoming of novel nanowires grown specifically for use in nanocrystal-based quantum electronics.

Chapter 5

Appendix

5.1 Complementary Visuals for the curious reader

In this chapter visual aids to the main text can be found – aptly named "Supplementary Figures." While not making the final cut of the thesis, these figures provide an additional look into the methods and findings of the work, without the bothersome clutter of words. It is said that a picture is worth thousands of words. Well then, these figures are worth at least a couple. Enjoy!

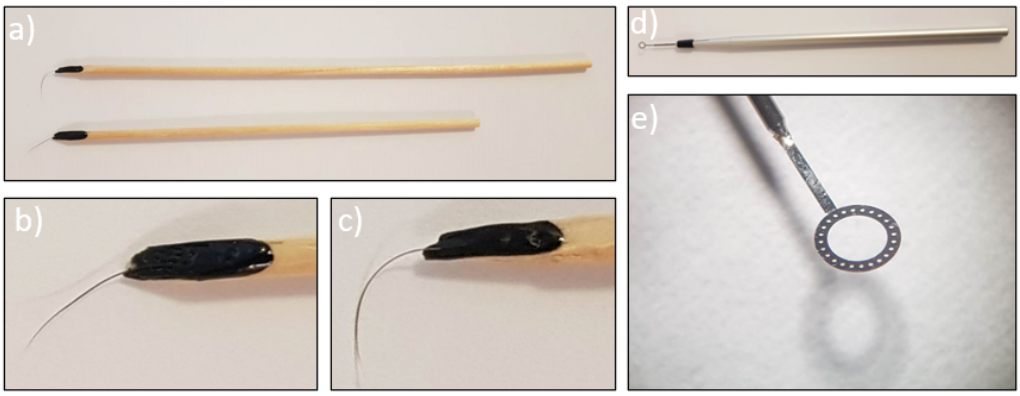

Figure 5.1: **Microtome cross-section tools.** a) Picture of two 'eyebrow'-rods. Top stick is a coarse tool and bottom is the gentle tool. b) Zoom in at the apex of the gentle tool. In this configuration the hair is mounted with the top of the brow oriented outward. c) Zoom in at the apex of the rough tool. Here the bottom part of the brow is oriented to point outward while the top is attatched to the stick. d) Perfect loop tool for transferring sections onto TEM grids. e) Magnified picture of the head part, used to transfer the sections.

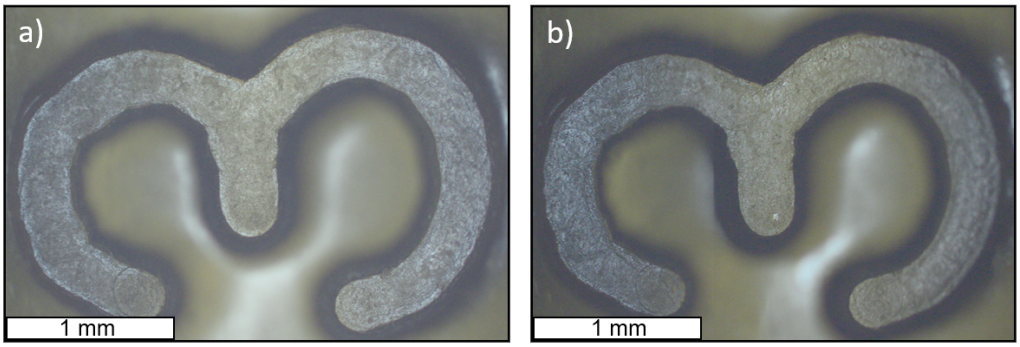

Figure 5.2: **Microtome resin test in butyl acetate.** Optical images of a microtome sample, zoomed in onto a surface detail. The sample was submerged into butyl acetate for 15 minutes to simulate the time a lamella will spend floating on the knifeboat medium before getting transfer ed to a sample. a) Sample before submerged in butyl acetate. b) Sample after submersion in butyl acetate .

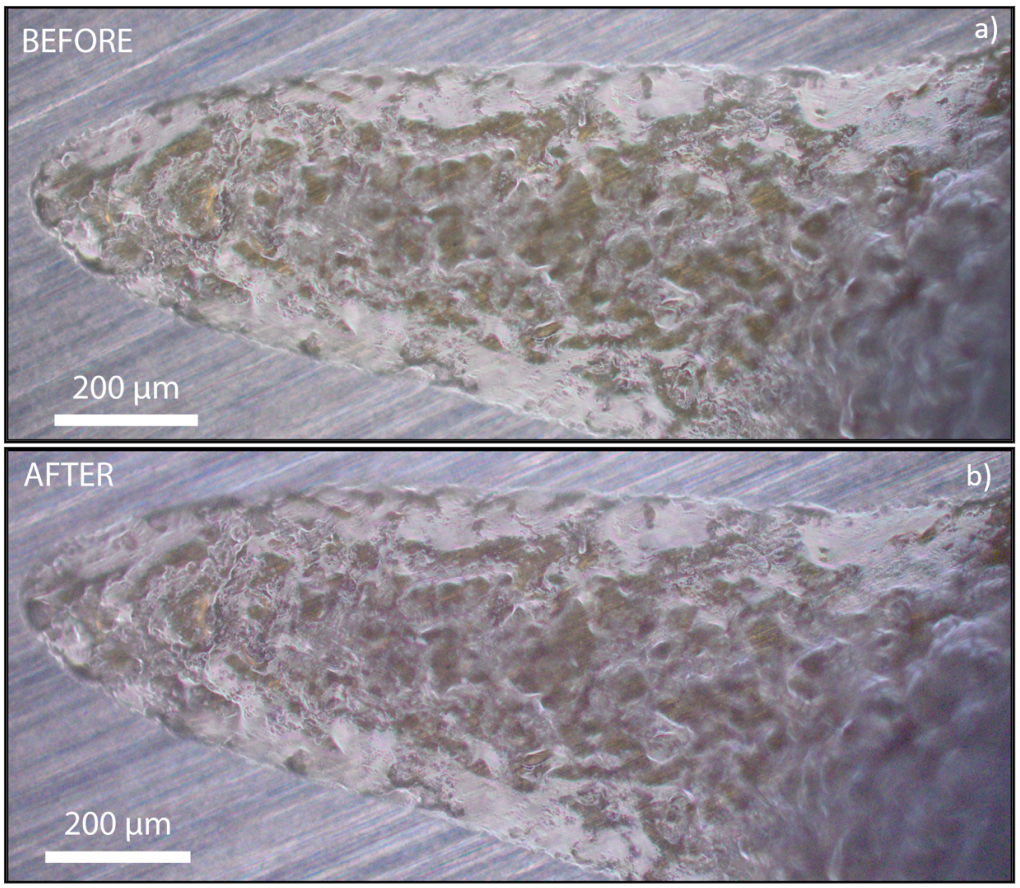

Figure 5.3: **Butyl acetate test on experimental knife holder epoxy.** Optical images of an epoxy, intended not to react with acetone. The sample was submerged into butyl acetate for 20 hours. a) The epoxy before being exposed to the butyl acetate. b) The epoxy after 20 hours submerged in butyl acetate, followed up with rinsing with MilliQ water and dried with nitrogen.

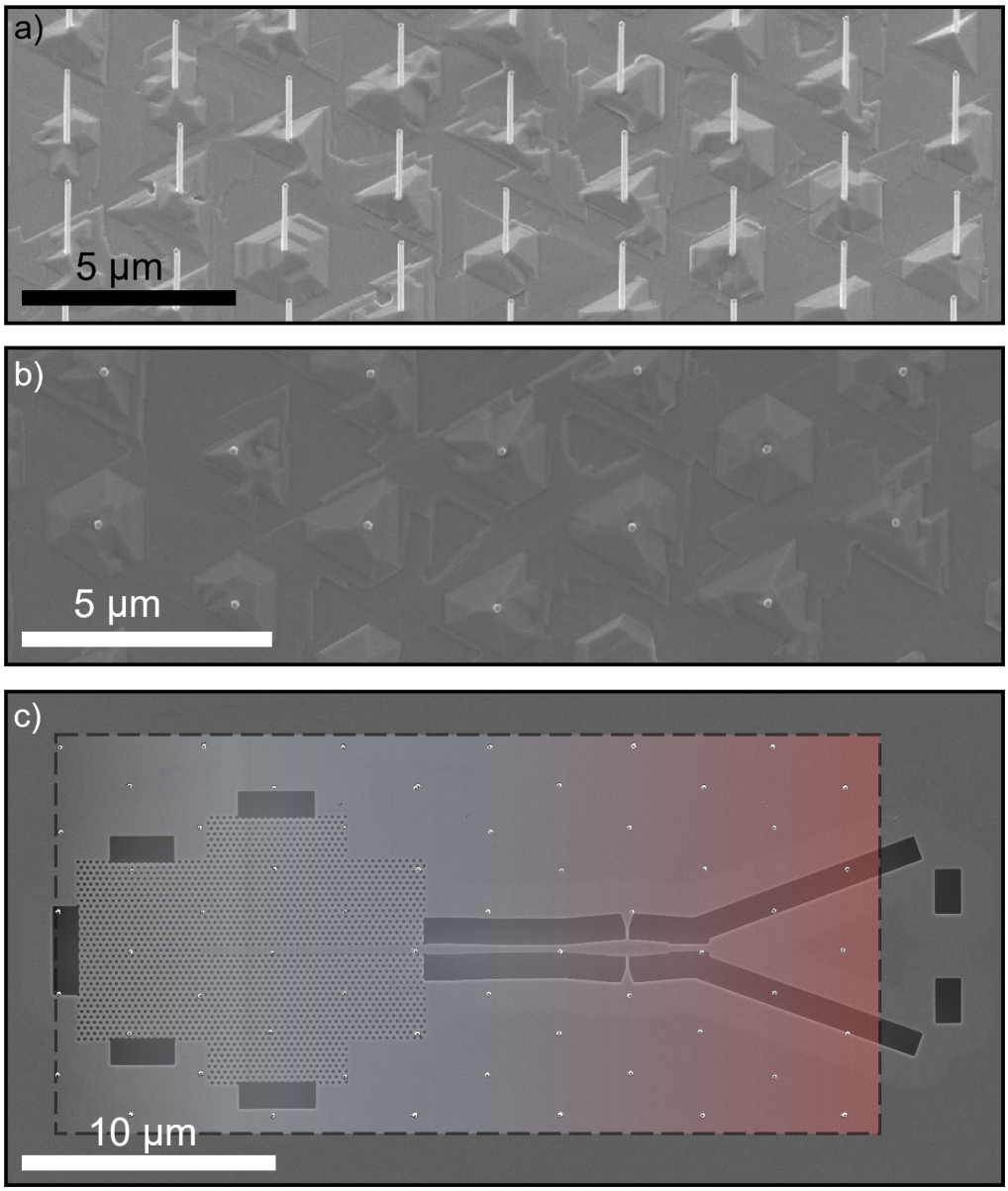

Figure 5.4: **Butyl acetate test on experimental knife holder epoxy.**a) SEM image of nanowire array tilted to view the full length of the wires. b) The same array of nanowires, seen from above with no tilt in order to illustrate the potential NCs. c) SEM image of a photonic device structure. In the dashed box and overlay of the wires in (b) is shown, as an example of how NCs can be transferred onto device locations.

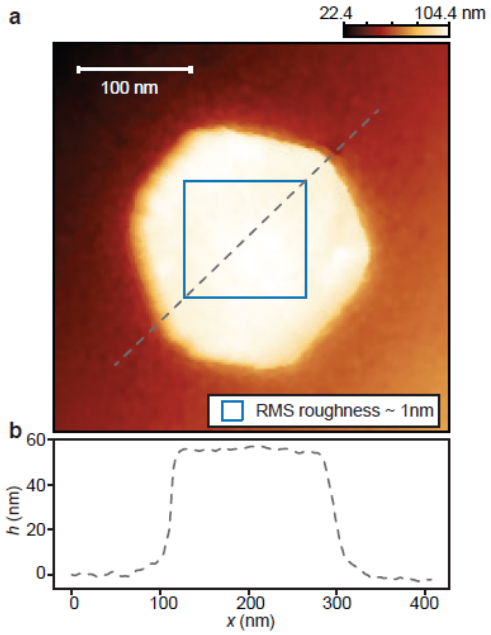

Figure 5.5: **AFM image of successfully sectioned/cleaved NC.** a) AFM image of NC extending $\sim$ 60 nm out from the lamella. The region marked by the blue square indicates the area from which the RMS roughness is calculated. b) Height versus path indicated by dashed line in a showing a flat topology of the NC. The figure and figure caption is published as supporting information to the article Ref.[17]

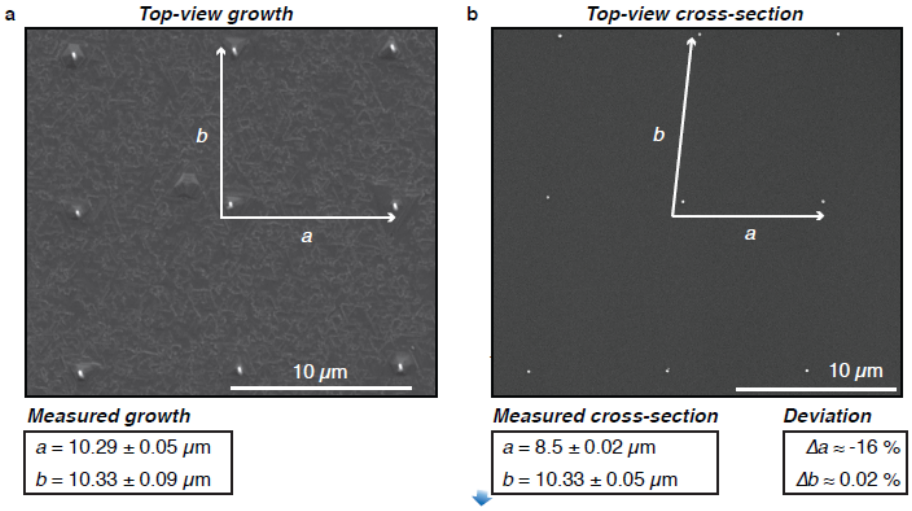

Figure 5.6: **Compression effects of the lamella during sectioning.** a) Top-view SEM image of as-grown nanowires. b) Top-view SEM image of the according nanocrystals after sectioning. The information boxes show the measured distances before/after sectioning and their deviation. The figure and figure caption is published as supporting information to the article [17].

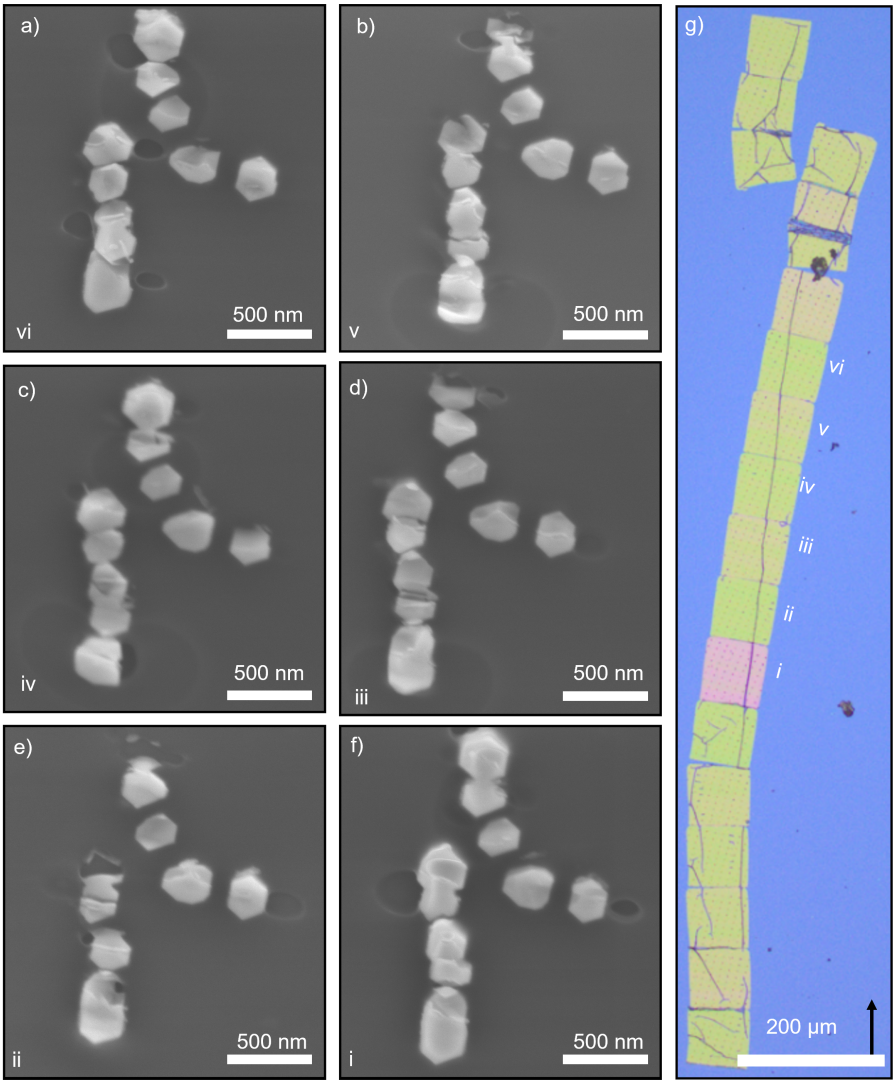

Figure 5.7: **NC configuration [a] across multiple consecutive increments.** a-f) SEM images of a NC structure created from the same nanowires at consecutive heights of the structure. moving down the length of the wire from (a) to (f). The index in the lower right show the order of which the NCs were performed aswell as the lamella on which they are located in the overview optical image in (g). The [a] in the tittle, indicates the position of the structure relative to the middle panel of Figure 3.9.

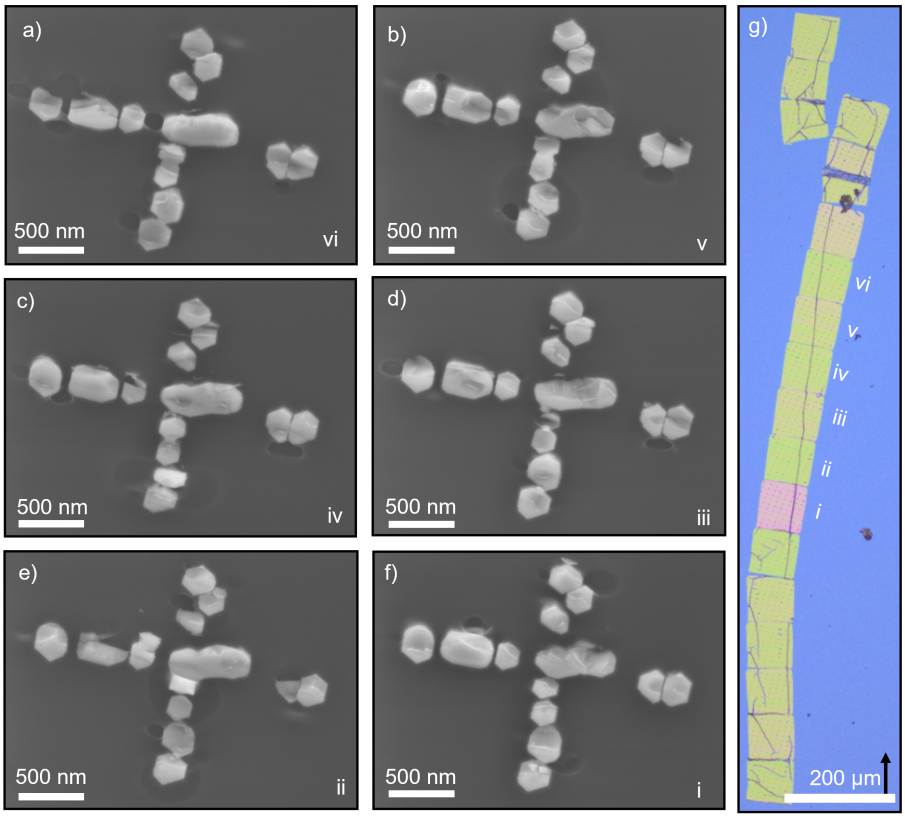

Figure 5.8: **NC configuration [b] across multiple consecutive increments.** a-f) SEM images of a NC structure created from the same nanowires at consecutive heights of the structure. moving down the length of the wire from (a) to (f). The index in the lower right show the order of which the NCs were performed aswell as the lamella on which they are located in the overview optical image in (g). The [b] in the tittle, indicates the position of the structure relative to the middle panel of Figure 3.9.

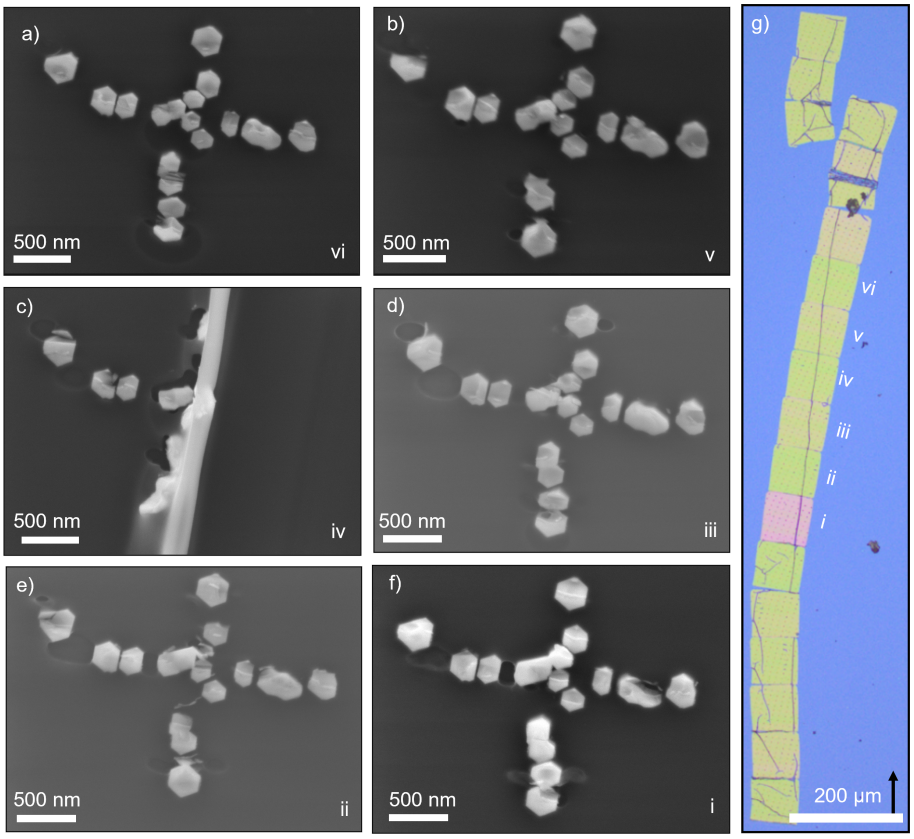

Figure 5.9: **NC configuration [c] across multiple consecutive increments.** a-f) SEM images of a NC structure created from the same nanowires at consecutive heights of the structure. moving down the length of the wire from (a) to (f). The index in the lower right show the order of which the NCs were performed aswell as the lamella on which they are located in the overview optical image in (g). The [c] in the tittle, indicates the position of the structure relative to the middle panel of Figure 3.9.

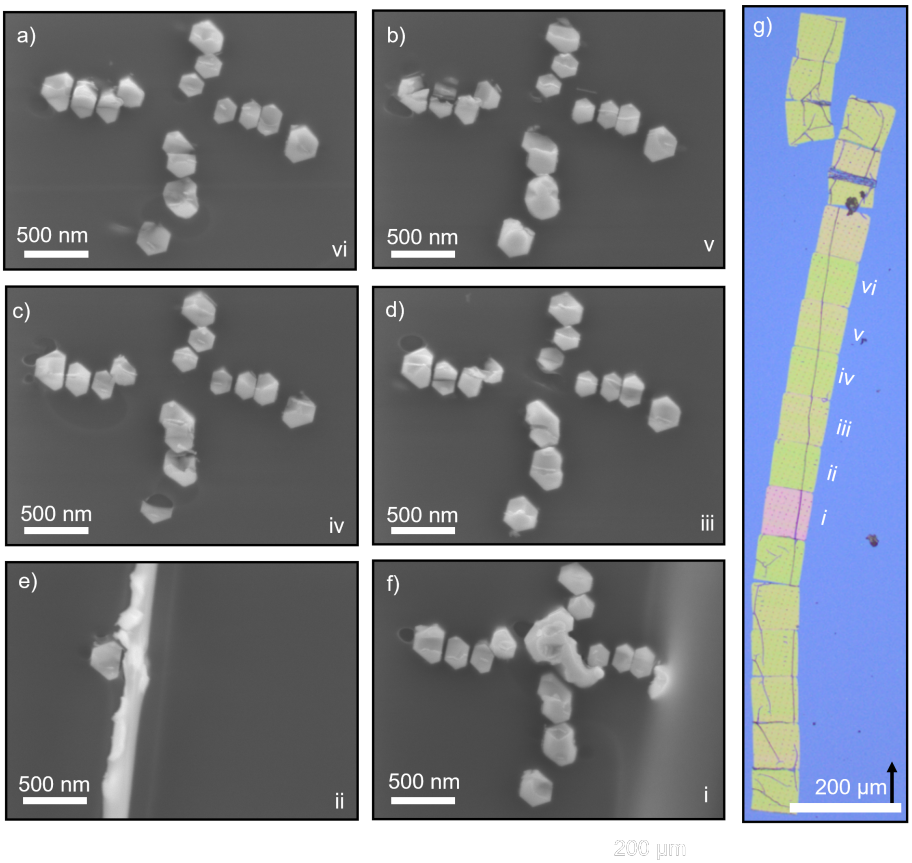

Figure 5.10: **NC configuration [e] across multiple consecutive increments.** a-f) SEM images of a NC structure created from the same nanowires at consecutive heights of the structure. moving down the length of the wire from (a) to (f). The index in the lower right show the order of which the NCs were performed aswell as the lamella on which they are located in the overview optical image in (g). The [e] in the tittle, indicates the position of the structure relative to the middle panel of Figure 3.9.

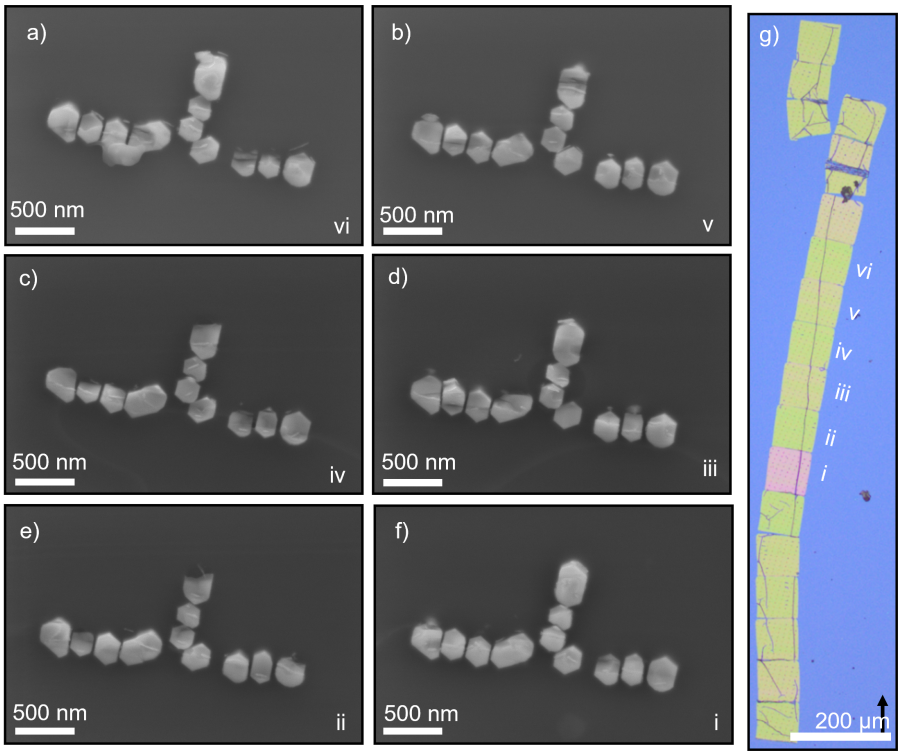

Figure 5.11: **NC configuration [f] across multiple consecutive increments.** a-f) SEM images of a NC structure created from the same nanowires at consecutive heights of the structure. moving down the length of the wire from (a) to (f). The index in the lower right show the order of which the NCs were performed aswell as the lamella on which they are located in the overview optical image in (g). The [f] in the tittle, indicates the position of the structure relative to the middle panel of Figure 3.9.

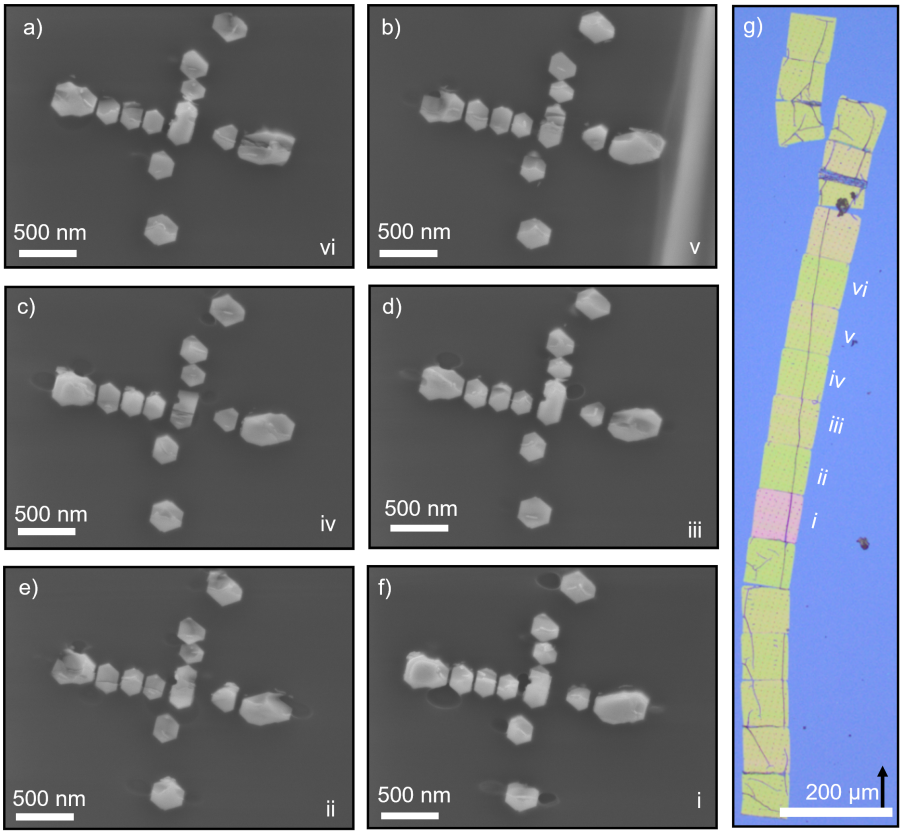

Figure 5.12: **NC configuration [g] across multiple consecutive increments.** a-f) SEM images of a NC structure created from the same nanowires at consecutive heights of the structure. moving down the length of the wire from (a) to (f). The index in the lower right show the order of which the NCs were performed aswell as the lamella on which they are located in the overview optical image in (g). The [g] in the tittle, indicates the position of the structure relative to the middle panel of Figure 3.9.

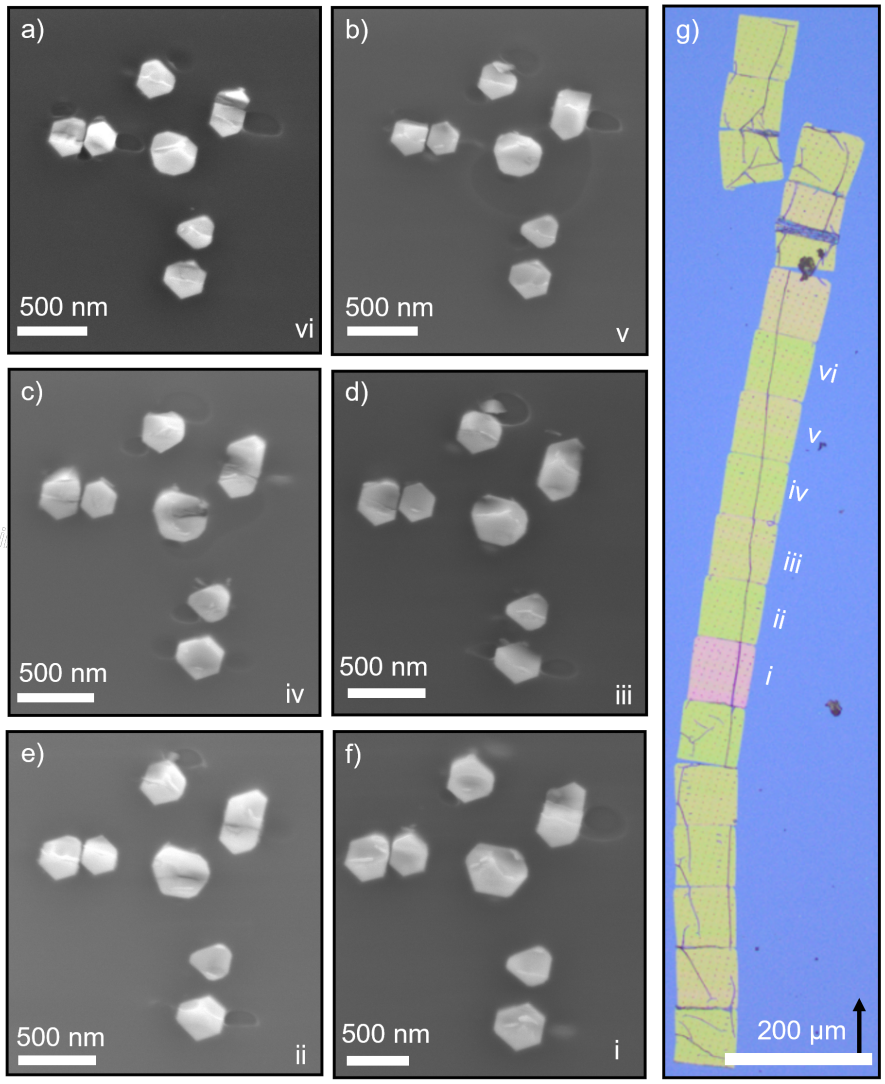

Figure 5.13: **NC configuration [h] across multiple consecutive increments.** a-f) SEM images of a NC structure created from the same nanowires at consecutive heights of the structure. moving down the length of the wire from (a) to (f). The index in the lower right show the order of which the NCs were performed aswell as the lamella on which they are located in the overview optical image in (g). The [h] in the tittle, indicates the position of the structure relative to the middle panel of Figure 3.9.

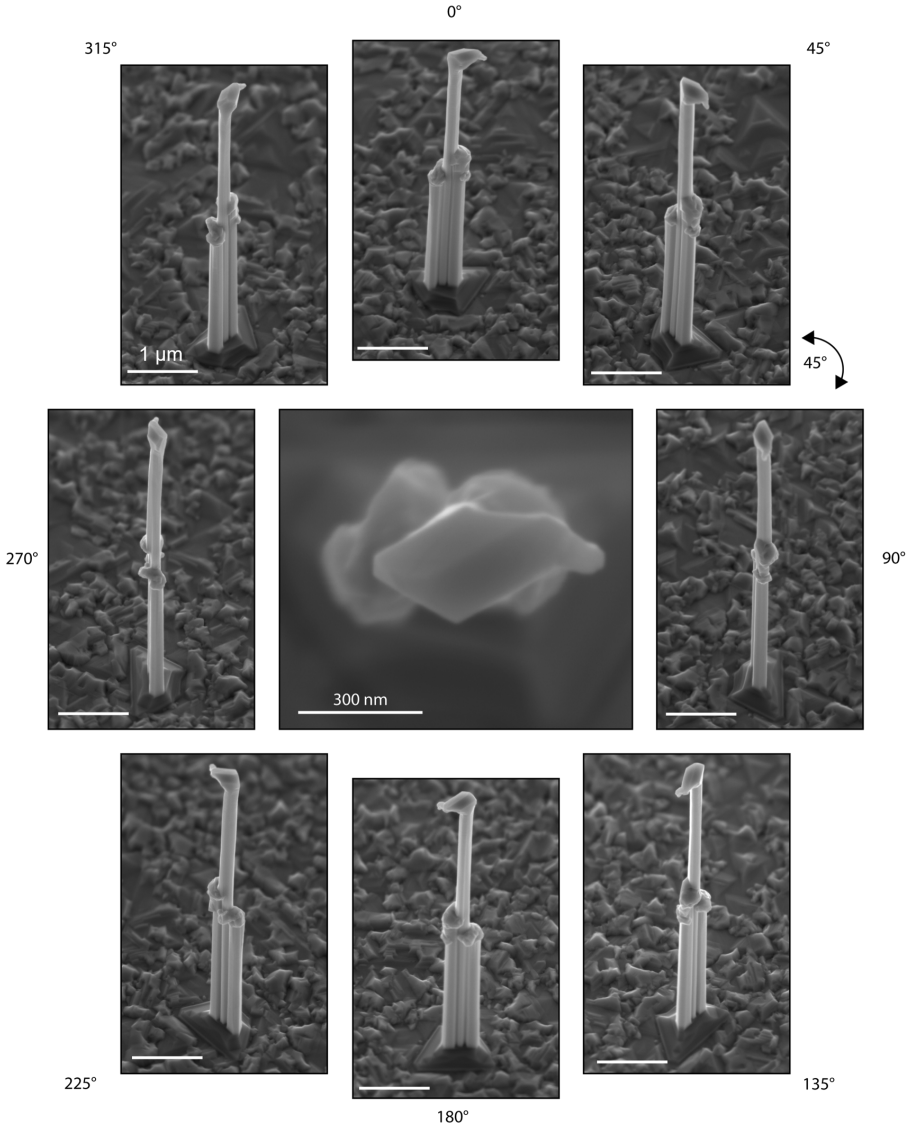

Figure 5.14: **Detailed investigation of structures prior to sectioning.** In the middle a SEM image is shown of a candidate structure. The sorounding frames are the same structure, seen along the length of the wire by tilting the sample holder by 45 degrees. The structure is investigated in rotation segments of 45 degrees. All the tilted images has a 1 µm scalebar.

Bibliography

1. Duan, X., Huang, Y., Cui, Y., Wang, J. & Lieber, C. M. Indium phosphide nanowires as building blocks for nanoscale electronic and optoelectronic devices. *nature* **409,** 66–69 (2001).
2. Cui, Y., Zhong, Z., Wang, D., Wang, W. U. & Lieber, C. M. High performance silicon nanowire field effect transistors. *Nano letters* **3,** 149–152 (2003).
3. Tian, B. *et al.* Coaxial silicon nanowires as solar cells and nanoelectronic power sources. *nature* **449,** 885–889 (2007).
4. Eaton, S. W., Fu, A., Wong, A. B., Ning, C.-Z. & Yang, P. Semiconductor nanowire lasers. *Nature reviews materials* **1,** 1–11 (2016).
5. Kanne, T. *et al.* Epitaxial Pb on InAs nanowires for quantum devices. *Nature Nanotechnology* **16,** 776–781 (2021).
6. Björk, M. T. *et al.* Tunable effective g factor in InAs nanowire quantum dots. *Physical Review B* **72,** 201307 (2005).
7. Zhang, H., Liu, D. E., Wimmer, M. & Kouwenhoven, L. P. Next steps of quantum transport in Majorana nanowire devices. *Nature communications* **10,** 5128 (2019).
8. Wagner, a. R. & Ellis, s. W. Vapor-liquid-solid mechanism of single crystal growth. *Applied physics letters* **4,** 89–90 (1964).
9. Fang, Z., Yan, Y. & Geng, Y. Recent progress in the nanoskiving approach: a review of methodology, devices, and applications. *Advanced Materials Technologies* **6,** 2100477 (2021).
10. Potts, H. *et al.* From Twinning to Pure Zincblende Catalyst-Free InAs(Sb) Nanowires. *Nano Lett.* **16,** 637–643 (2015).

11. Watson, D. C. *et al.* Nanoskiving Core–Shell Nanowires: A New Fabrication Method for Nano-optics. *Nano Lett.* **14,** 524–531 (2014).

12. Yuan, X., Caroff, P., Wong-Leung, J., Tan, H. H. & Jagadish, C. Controlling the morphology, composition and crystal structure in gold-seeded GaAsSb nanowires. *Nanoscale* **11,** 4995–5003 (2015).

13. Saxena, D. *et al.* Design and Room-Temperature Operation of GaAs/AlGaAs Multiple Quantum Well Nanowire Lasers. *Nano Lett.* **16,** 5080–5086 (2016).

14. Tambe, M. J., Allard, L. F. & Gradecak, S. Characterization of core-shell GaAs/AlGaAs nanowire heterostructures using advanced electron microscopy. *J. Phys.: Conf. Ser.,* 012033 (2010).

15. Zheng, C. *et al.* Polarity-Driven 3-Fold Symmetry of GaAs/AlGaAs Core Multishell Nanowires. *Nano Lett.* **13,** 3742–3748 (2013).

16. Fonseka, H. A. *et al.* Self-Formed Quantum Wires and Dots in GaAsP–GaAsP Core–Shell Nanowires. *Nano Lett.* **19,** 4158–4165 (2019).

17. Sestoft, J. E. *et al.* Scalable Platform for Nanocrystal-Based Quantum Electronics. *Adv. Funct. Mater.* **32,** 2112941 (2022).

18. Williams, D. B. & Carter, C. B. *Transmission Electron Microscopy - A Textbook for Materials Science* ISBN: 9780387765006 (Springer New York, 2009).

19. *Spurr Low Viscosity Embedding Kit* `https://www.sigmaaldrich.com/DK/en/product/sigma/em0300`. (accessed: 11.03.2023).

20. *Spurr Low Viscosity Embedding Kit (EM0300)* `https://www.sigmaaldrich.com/deepweb/assets/sigmaaldrich/product/documents/274/487/em0300bul.pdf`. (accessed: 11.03.2023).

21. Trayner, S. *Improvement of microtome cutting process of carbon nanotube composite sample preparation for TEM analysis* in (2014).

22. *Perfect loop* `https://www.diatome.ch/en/products/perfectloop.asp`. (accessed: 12.03.2023).

23. Dubrovskii, V. G. *Nucleation theory and growth of nanostructures* (Springer, 2014).

24. Kanne, T. *et al.* Epitaxial Pb on InAs nanowires for quantum devices. *Nature Nanotechnology.* **16,** 776–781 (2021).

25. Krogstrup, P *et al.* Epitaxy of semiconductor–superconductor nanowires. *Nature Materials* **14,** 400 (Jan. 2015).